Supplementary Information for:

Tuning the Baird aromatic triplet state energy of cyclooctatetraene to maximize the self-healing mechanism in organic fluorophores

Avik K Pati[a,b], Ouissam El Bakouri[c,1], Steffen Jockusch[d,1], Zhou Zhou[a,1], Roger B Altman[a,b], Gabriel A Fitzgerald[a], Wesley B Asher[e,f,g], Daniel S Terry[a,b], Alessandro Borgia[b], Michael D Holsey[e,f], Jake E Batchelder[a,b], Chathura Abeywickrama[b], Brandt Huddle[a], Dominic Rufa[a], Jonathan A Javitch[e,f,g], Henrik Ottosson[c], and Scott C Blanchard[a,b,2]

[a]Department of Physiology and Biophysics, Weill Cornell Medicine, New York, NY 10065;

[b]Department of Structural Biology, St. Jude Children's Research Hospital, Memphis, TN 38105;

[c]Ångström Laboratory, Department of Chemistry, Uppsala University, Uppsala, 751 20 Sweden;

[d]Department of Chemistry, Columbia University, New York, NY 10027;

[e]Department of Psychiatry, Columbia University, New York, NY 10032;

[f]Department of Pharmacology, Columbia University, New York, NY 10032; and

[g]Division of Molecular Therapeutics, New York State Psychiatric Institute, New York, NY 10032

[1]O.E.B., S.J., and Z.Z. contributed equally to this work.

[2]Correspondence should be addressed to S.C.B.: scott.blanchard@stjude.org.

Supplementary Figure 1	Molecular structures of parent and self-healing cyanine fluorophores and other cyanine and rhodamine dyes
Supplementary Figure 2	^{1}H NMR of COT molecules and retention times of parent and self-healing cyanine fluorophores and other cyanine and rhodamine dyes
Supplementary Figure 3	Ring inversion rates, aromaticity indicators and impact of triplet state COT ring strain on self-healing fluorophore photostability
Supplementary Figure 4	Transient absorbance of parent and self-healing cyanine fluorophores
Supplementary Figure 5	Fluorescence quantum yield, fluorescence lifetime, radiative and nonradiative rate constants, and cis state population of parent and self-healing cyanine fluorophores
Supplementary Figure 6	Reactive oxygen species generation and bulk photostability of parent and self-healing cyanine fluorophores
Supplementary Figure 7	Impact of BME on the photostability of parent and self-healing cyanine fluorophores
Supplementary Figure 8	Photon count rates at high time resolution (1 ms) for parent and self-healing cyanine fluorophores and other cyanine and rhodamine dyes
Supplementary Figure 9	Photophysical evaluation of parent cyanine fluorophores in the absence and presence of solution additives and self-healing cyanine fluorophores (no additive)
Supplementary Figure 10	Blinking characterization of parent and self-healing cyanine fluorophores
Supplementary Figure 11	Comparative photophysical evaluation of self-healing fluorophores and other cyanine and rhodamine dyes in the absence of solution additives
Supplementary Figure 12	Comparative photophysical evaluation of self-healing fluorophores (no additive) and other cyanine and rhodamine dyes in the absence and presence of solution additives with no supplementary BME
Supplementary Figure 13	Comparison of single-molecule fluorescence traces of self-healing cyanine and rhodamine dyes
Supplementary Figure 14	smFRET experiments of self-healing cyanine fluorophores labeled LIV-BP^{SS}
Supplementary Figure 15	Comparisons of smFRET experiments of self-healing cyanine fluorophores and other cyanine and rhodamine dyes labeled LIV-BP^{SS}
Supplementary Figure 16	Assessments of cytotoxicity with commonly used photoprotective agents for biological imaging
Supplementary Figure 17	Evaluations of non-specificity and photobleaching times of self-healing cyanine fluorophores and other cyanine and rhodamine dyes in living-cells
Supplementary Table 1	Triplet energies (E_T), inversion barriers (ΔE_{inv}), energy difference between the optimal triplet state and the planar singlet state ($\Delta E_{TS(S0) \rightarrow T1ad}$), energy for vertical excitation from the planar singlet state to the triplet state ($\Delta E_{TS(S0) \rightarrow T1vert}$), vertical emission energies from the optimal triplet state structure to the singlet state ($\Delta E_{T1ad \rightarrow S0}$), triplet state ring distortion energy, and ground state HOMO energy of COT molecules [A simplified schematic of the aforementioned various energies is displayed at the top of the table]
Supplementary Table 2	Computed Gibbs energy (ΔG) of reaction of triplet state quenchers (TSQs) with molecular oxygen
Supplementary Table 3	Quantitative photophysical parameters of parent and self-healing cyanine fluorophores
Supplementary Information for Synthesis	Synthetic details and characterizations of cyanine fluorophores
Supplementary Video 1	Photostability of Cy3 fluorophores when linked to DNA duplexes in deoxygenated buffers. Shown are single-molecule TIRF movies of Cy3 parent (top left), Cy3-4S-

	Me-COT (top right), Cy3-4S-AC (bottom left), Cy3-4S-DAC (bottom right) taken at 100 ms time resolution.
Supplementary Video 2	Photostability of Cy5 fluorophores when linked to DNA duplexes in deoxygenated buffers. Shown are single-molecule TIRF movies of Cy5 parent (top left), Cy5-4S-Me-COT (top right), Cy5-4S-AC (bottom left), Cy5-4S-DAC (bottom right) taken at 100 ms time resolution.
Supplementary Video 3	Photostability of Cy7 fluorophores when linked to DNA duplexes in deoxygenated buffers. Shown are single-molecule TIRF movies of Cy7 parent (top left), Cy7-4S-Me-COT (top right), Cy7-4S-AC (bottom left), Cy7-4S-DAC (bottom right) taken at 100 ms time resolution.
Supplementary Video 4	Photostability of Cy3 fluorophores when linked to DNA duplexes in oxygenated buffers. Shown are single-molecule TIRF movies of Cy3 parent (top left), Cy3-4S-Me-COT (top right), Cy3-4S-AC (bottom left), Cy3-4S-DAC (bottom right) taken at 100 ms time resolution.
Supplementary Video 5	Photostability of Cy5 fluorophores when linked to DNA duplexes in oxygenated buffers. Shown are single-molecule TIRF movies of Cy5 parent (top left), Cy5-4S-Me-COT (top right), Cy5-4S-AC (bottom left), Cy5-4S-DAC (bottom right) taken at 100 ms time resolution.
Supplementary Video 6	Photostability of Cy7 fluorophores when linked to DNA duplexes in oxygenated buffers. Shown are single-molecule TIRF movies of Cy7 parent (top left), Cy7-4S-Me-COT (top right), Cy7-4S-AC (bottom left), Cy7-4S-DAC (bottom right) taken at 100 ms time resolution.

Note: Cartesian co-ordinates and absolute energies of all computationally optimized molecules are available from the authors upon request.

Supplementary Methods

Preparation of dye-labeled DNA duplexes

A 21-nucleotide DNA, 5′-(5AmMC6)CATGACCATGACCATGACCAG(3BioTEG)-3′, containing a 5′ amino modifier with a six-carbon linker (5AmMC6) for fluorophore linkage and an additional 3′ biotin moiety attached via a 22-atom tetra-ethylene glycol (TEG) spacer (3BioTEG) was purchased from Integrated DNA Technologies along with a complementary DNA strand (5′-CTGGTCATGGTCATGGTCATG-3′). 1 nmol of the 5'-amino modified DNA was individually labeled with 10-fold excess of N-hydroxysuccinimide (NHS) ester-activated fluorophore in a 10 μL final reaction containing 50 mM potassium borate (pH 8.1), 200 mM KCl, and 10% DMSO. After incubation at 23° C for 1hr, the reaction mixture was subsequently quenched with 0.2 μL of 1 M Tris-acetate (pH 7.5) at 23° C for 2 min before addition of the complementary strand in an equimolar ratio and heated at 90° C for 2 minutes followed by passive cooling to room temperature (23° C). 80 μL ddH_2O and 10 μL of 3M sodium acetate (pH 6) were then added followed by 3-fold excess of ethanol for precipitation of the duplexes. The resulting pellet from a 10 minute spin at 14,000 rpm was resuspended in 1 ml of buffer A (1.7 M ammonium sulfate, 10 mM ammonium acetate, pH 5.8) and injected onto a phenyl 5PW column (FPLC, Äkta Purifier, GE Healthcare) and eluted over a 30-min gradient from buffer A to B [10% methanol and 10 mM ammonium acetate (pH 5.8) for green and red dyes; and 30% methanol and 10 mM ammonium acetate (pH 5.8) for near-infrared dyes]. The desired peak of interest was collected, stored at –80^{o} C and used for single-molecule investigations.

Quantum chemical computations

All geometry optimizations were performed with Gaussian 16 at the M062X/6-31+G(d) level (1, 2). The triplet energies are adiabatic and computed as the energy differences between the singlet ground state and the first triplet state at their optimal geometries. The triplet energies of the COT molecules and parent cyanine dyes, and the ring inversion barrier energies of the COT molecules in ground states that were compared with experimental results were calculated from the gas-phase Gibbs free energies by adding the Gibbs solvation energies in ethanol obtained through single-point energy calculations with the polarizable continuum model (PCM) at the M062X/6-311+G(d,p)//M062X/6-31+G(d) and OLYP-D3/6-311+G(d,p)//OLYP-D3/6-31+G(d) level of theories (2–7) respectively, unless otherwise specified. We used M062X computed results as it gave the best agreement with experimentally determined triplet energy for the cyanines, whereas OLYP gave best agreement with the experimentally determined ring inversion energy for COT. The computed ring inversion energies were used to calculate ring inversion time using Eyring equation (8). The triplet state ring distortion energies were calculated by considering the structural distortions of the carbon framework of a triplet state COT molecule relative to those in the optimal geometries of amide-substituted COT molecules using M062X/6-31+G(d) level of theory in gas phase. The HOMO energies were computed at the M062X/6-31+G(d) and M062X/6-311+G(d,p) level in gas phase.

Aromaticity was evaluated in terms of geometric, electronic, and magnetic indices for which we used the harmonic oscillator model of aromaticity (HOMA) (9–11), the multicenter index (MCI) (12), the aromatic fluctuation index (FLU) (13) and the nucleus-independent chemical shifts (NICS) (14), respectively in gas phase. In the latter case, NICS-Z scans were made using the Aroma package (15–17). As a magnetic descriptor, anisotropy of induced current density (ACID) plots were also computed (18, 19). All MCI and FLU calculations were carried out with the ESI-3D program (20) using the QTAIM (Quantum Theory of Atoms in Molecules) atomic partition and

the integration scheme as implemented in the AIMAll package (21). The Gibbs energies (ΔG) of reactions of TSQs with molecular oxygen were computed using the B3LYP and M062X functionals (2, 6, 22), and the G3MP2B3 (23) and G4MP2 (24) composite methods in gas phase.

The quantum chemical calculations of parent COT and amide-substituted COT molecules were performed on their methylated derivatives to recapitulate the context when they are intramolecularly linked to fluorophores. The triplet energy calculations of cyanine dyes were performed on parent Cy3, Cy5 and Cy7 fluorophores. Our theoretical triplet energy data of Cy5 (144.9 kJ/mol) closely matched with our earlier measured triplet energy data (143.6 kJ/mol) of Cy5 fluorophore (25). We measured the triplet state energy of Cy3 fluorophore (165.23 kJ/mol), and it closely matched with our theoretical data (173.8 kJ/mol). However, we could not measure the triplet energy of a Cy7 fluorophore using the phosphorescence technique (25), presumably because of its relatively low phosphorescence quantum yield due to its lower singlet-triplet energy gap that increases the rate of intersystem-crossing from the triplet to singlet ground state, as well as the reduced quantum efficiency of our detectors in this region of the visible spectrum.

Triplet state lifetime measurements

Triplet state lifetimes of the OTX-conjugated cyanine fluorophores were measured with a home-built laser flash photolysis setup using a Nd:YAG laser (355 nm, 5 ns pulse width) and a computer controlled system, as described earlier (26). Acetonitrile solutions of the cyanine dyes with covalently attached triplet sensitizer, OTX, were deoxygenated prior to experiments. The laser pulses at 355 nm generated excited states of OTX which, after intersystem crossing, undergoes intramolecular triplet energy transfer to the cyanine dyes. All the measurements were carried out using 10 x 10 mm quartz cell and right-angle pump-probe geometry.

Single-molecule fluorescence imaging of dyes bound to DNA oligonucleotides

The single-molecule fluorescence imaging experiments were performed using a custom-built, prism-based total internal reflection fluorescence (TIRF) microscope, as described previously (27). Fluorophores containing biotinylated DNA molecules were immobilized *via* biotin-streptavidin interactions in quartz microfluidic chambers. Fluorescence from the surface-immobilized dyes, illuminated by the evanescent wave generated by total internal reflection of laser light, was collected using a 1.27 numerical aperture (NA), 60X water-immersion objective (Nikon) and imaged onto a scientific complementary metal-oxide semiconductor (sCMOS) camera (Hamamatsu ORCA-Flash 4.0 v2) having 2,048 × 2,048 pixels with 6.5-μm pixel size, connected to a PC with Camera Link acquisition boards and 2x2 binning.

Experiments were performed in T50 buffer, made using 10 mM Tris HCl (pH 7.4), 50 mM KCl at 25 ^{o}C, unless otherwise specified. The experiments were performed either in the absence or in the presence of BME (0.1 mM BME for Cy3 and Cy7 derivatives; and 2 mM BME for Cy5 derivatives). The experiments in deoxygenated conditions were performed by using 1 mM 3,4-dihydroxybenzoic acid (PCA) and 50 nM protocatechuate 3,4-deoxygenase (PCD) (Sigma-Aldrich) as oxygen scavengers. Experiments were performed with a direct excitation of the fluorophores. The experiments of Cy3, Cy5, and Cy7 class of dyes were carried out with a single-frequency laser at 532 nm (Opus, Laser Quantum); 639 nm (Genesis MX-STM; Coherent); and 721 nm (Laser Glow), respectively. Unless otherwise specified, experiments in deoxygenated imaging buffers at 100 ms time resolution were performed at excitation intensities 70 W/cm^2 for Cy3 derivatives and 180 W/cm^2 for Cy5 and Cy7 derivatives. The experiments in oxygenated imaging buffers at 100 ms time resolution were performed at excitation intensities 70, 20 and 60 W/cm^2 for Cy3, Cy5 and Cy7 derivatives, respectively unless otherwise specified. The experiments of all commercially obtained green, red and NIR dyes were carried out at the same experimental conditions that were used for Cy3, Cy5 and Cy7 class of dyes, respectively unless

otherwise specified. All movies were recorded using custom software implemented in LabView (National Instruments).

Single-molecule imaging data analysis of dye labeled DNA oligonucleotides

Analysis of wide-field TIRF movies was performed using SPARTAN (Single-molecule Platform for Automated Analysis) software (27) implemented in MATLAB. Single-molecules were detected within wide-field TIRF movies by finding peaks of fluorescence signal at least 8 standard deviations above background noise. Peaks that are closer than 3.5 pixels were automatically removed. Single-molecule traces were then extracted by summing the 9 most intense pixels within the 5x5 pixel neighborhood around each peak of intensity, applying a scaling factor provided by the camera vendor for converting from the camera's arbitrary units to photon counts (0.49 photoelectrons per ADU). Further, we applied a set of selection criteria for 100 ms time resolution measurements*:* signal-to-background noise ratio >10, background noise level within 4 standard deviation of the mean, and single photobleaching step to reduce analytical errors. The field of view was illuminated with a Gaussian-shaped beam in which the edges of the field had lower illumination intensities than the center. In order to analytically minimize the contributions from this non-uniformity, we selected for analysis only molecules within the center proportion of the field (25% total area) for all 100 ms time resolution measurements.

For determinations of fluorophore lifetime before photobleaching, we idealized fluorescence traces using the segmental *K*-means (SKM) algorithm (28) after normalizing to the mean fluorescence intensity. A three-state model with one fluorescent (ON) state, a transient dark state corresponding to fluorophore blinking and a permanent dark state due to fluorophore photobleaching was used for the data analysis. Any trace with more than two standard deviations from the mean in the number of transitions was removed from analysis to avoid molecules with aberrant behavior. We calculated the ON state lifetime (τ_{ON}) by fitting the cumulative distribution of fluorescence intensity (survival plot) to an exponential function. Total τ_{ON} prior to fluorophore

photobleaching was calculated by taking the mean of the distributions of the total time spent in the ON state in each trace. Total photon budgets were calculated by multiplying total τ_{ON} with the mean of the distribution of detected photons detected per frame in each trace. Traces for 1 ms time resolution measurements were selected based on the criteria*:* signal-to-background noise ratio >8, background noise level <70, and single photobleaching step.

Bulk fluorescence lifetime and quantum yield measurements

Bulk fluorescence measurements were carried out in a FluoTime 300 steady-state and lifetime spectrometer (PicoQuant GmbH, Berlin). Steady-state fluorescence spectra of the dyes were recorded using a 300 W xenon lamp. Fluorescence lifetimes of Cy3, Cy5 and Cy7 class of dyes were measured using 530 (LDH-P-FA-530B), 640 (LDH-D-C-640) and 730 (LDH-D-C-730) nm pulsed diode lasers (PicoQuant GmbH, Berlin), respectively. The instrument response function (IRF) was collected using a scatterer (Ludox AS40 colloidal silica, Sigma-Aldrich). The TCSPC data from the fluorescence lifetime measurements were fitted into an exponential decay model in EasyTau software (PicoQuant GmbH, Berlin). A value of χ^2, in between 0.98 and 1.2, was considered as a good fit, which was further adjudged by symmetrical distribution of the residuals. Fluorescence lifetimes of Cy3, Cy5 and Cy7 derivatives were collected at emission wavelengths 570, 670 and 780 nm, respectively.

Absolute fluorescence quantum yields of the cyanine dyes were measured in a FluoTime 300 spectrometer using integrating sphere accessories (PicoQuant GmbH, Berlin) and a 300 W xenon excitation lamp. Cy3, Cy5 and Cy7 derivatives were photoexcited at 517, 580 and 680 nm; and the detection ranges were 512–700, 575–800 and 675–835 nm, respectively. Prior to the quantum yield measurements, absorbance of the dyes at the excitation wavelengths was adjusted to 0.02 in a Shimadzu UV-2600 spectrometer, to minimize re-absorption of emitted photons. All these bulk measurements were carried out with free cyanine dyes in water at room temperature using standard 1 cm path length quartz cuvettes (Starna Cells, Inc.). The absorption and emission

maximum wavelengths, fluorescence quantum yield and fluorescence lifetime values of all the cyanine derivatives are tabulated in **Supplementary Table 3**.

Bulk photostability experiments

Bulk photobleaching experiments of free cyanine dyes were carried out in a 1 cm cuvette containing 2 mL of fluorophore solution in water at 23 ^{o}C. The samples were illuminated for fixed periods of time with a 300 W tungsten halogen lamp. Experiments of Cy5 and Cy7 derivatives were carried out in conjunction with a RG570 long pass filter. After each photolysis period, the absorbance was measured with a UV–vis spectrometer (Agilent 8453). The decrease in the absorption was used to estimate the rate of fluorophore photobleaching using a linear fit. The relative photobleaching rates were calculated with respect to individual parent dyes.

Measurements of reactive oxygen species

Reactive oxygen species (ROS) generation by the cyanine dyes upon photoexcitation was measured using 3,3'-diaminobenzidine (DAB) as an optical sensor. Generated ROS by the cyanine dyes oxidized DAB that was measured as an increase in absorbance of DAB at 400 nm (29). Cy3, Cy5 and Cy7 derivatives containing 200 μM DAB were illuminated with 550, 650 and 750 nm wavelength of light, respectively by a 300 W xenon lamp in a FluoTime 300 spectrophotometer (PicoQuant GmbH, Berlin) set up. Prior to illumination, the absorbance of all the dyes at their individual illumination wavelength was adjusted to 1.2. The absorbance at 400 nm was monitored using a Shimadzu UV-2600 spectrometer before the illumination and after illumination over fixed intervals of time. The starting optical density at 400 nm was adjusted to zero. The change in absorbance values with illumination time was fitted into a linear equation, in which the slope indicated the rate of ROS generation. The ROS generation rates of the self-healing dyes were estimated relative to the individual parent dyes. All these photoreactions were

carried out with free cyanine dyes in water at room temperature using standard 1 cm path length quartz cuvettes (Starna Cells, Inc.) and a solution volume of 2 mL.

Measurements of cis-trans isomerization by fluorescence correlation spectroscopy

Measurements of cis-trans isomerization of the cyanine dyes were carried out using fluorescence correlation spectroscopy (FCS) (30) in a MicroTime 200 time-resolved confocal fluorescence microscope (PicoQuant GmbH, Berlin). Cy3, Cy5 and Cy7 class of dyes were photoexcited by a laser beam from 530 (LDH-P-FA-530B), 640 (LDH-D-C-640) and 730 (LDH-D-C-730) nm pulsed diode lasers (PicoQuant GmbH, Berlin), respectively. The beam from the laser source was reflected by a main dichroic mirror [ZT 532/640 rpc-UF3, Chroma (for Cy3 and Cy5), or ZT 532-730 rpc-UF3 (for Cy7)] and then focused by a water immersion 60X microscope objective with numerical aperture (NA) 1.2 (Olympus IX 83). The fluorescence signal from the sample was collected by the same objective and passed through the same main dichroic mirror to a pinhole (radius 50 μm). Right before the pinhole, a band-pass filter was placed [582/64, Semrock (for Cy3), or H690/70, Semrock (for Cy5) or 810/90, Semrock (for Cy7)] to block scattered laser light and allow only the fluorescence signal to pass. The fluorescence photons were detected by two single-photon avalanche photodiodes (Excelitas technologies, model SPCM-AQRH-14-TR). The output signals as well as the trigger signals from Sepia II laser diode driver (PDL 828, PicoQuant GmbH, Berlin) were collected by a dedicated multichannel picosecond event timer and time-correlated single-photon counting (TCSPC) module (HydraHarp 400, PicoQuant GmbH, Berlin).

All these FCS experiments were carried out with cyanine dyes bound to DNA oligonucleotides in presence of oxygen and at room temperature in diffusion condition. A droplet (~20 μL) of the samples (concentration ~1 nM) prepared in T50 buffer containing 10 mM Tris HCl (pH 7.4) and 50 mM KCl was placed on the top of a clean glass coverslip. The T-50 buffer was supplemented with 0.1 mM BME for Cy3 and Cy7 class of dyes; and 2 mM BME for

Cy5 derivatives. The water immersion objective was focused 20 µm into the solution. Relatively low excitation power (2 µW for Cy3 and Cy7, and 1 µW for Cy5 derivatives) was used for the experiments to avoid the formation of triplet states. The cross-correlated data were fitted into two state models corresponding to diffusion and dark cis state (diffusion model alone did not produce good fit) using SymPhoTime 64 software (PicoQuant GmbH, Berlin). The formation of cis state was confirmed by performing experiments in a viscous solvent mixture (50% glycerol in T-50).

Cell viability assessments

For cell viability screening, HEK293H cells were cultured with Dulbecco's modified Eagle's medium (DMEM) (Invitrogen) containing 10% FBS and 1% Penstrep and incubated at 37ºC in a 5% CO_2 humidified incubator. Cells were treated with TSQ compounds dissolved in DMSO. TSQ treated cells were incubated for 2 hours at 37 ºC. DMSO (0.25%) was used as the negative control and Staurosporine (5 µM) was used as the positive control.

For Promega CellTiter-Glo® Luminescent assays, cells were seeded in Corning™ 96 well opaque bottom, tissue culture treated microplates (1,500 cells per well) prior to TSQ treatment. Cell viability experiments were carried out according to the standard manufacturer's protocol. Luminescence readings were recorded by using Spectramax® iD5 microplate reader by using default Spectramx® software installed for CellTiter Glow viability test protocol.

For Immunofluoresence assays, cells were seeded in 24-well plates prior to TSQ treatment followed by immunofluorescence protocol as performed previously (31). DAPI (Cat. 268298, Millipore and Phalloidin (Cat. 00043, Biotium) reagents, as well as α-cleaved-Caspase-3 (Cat. 9661, Cell Signaling Technology) and α-Rabbit IgG (Cat. A21244, Life Technologies) antibodies, were used according to manufacturer's instructions. Images were captured by a Zeiss Axioscan slide scanner.

LIV-BP^{SS} expression, purification and labeling

A His-tagged LIV-BP^{SS} construct, generously provided by Dr. Mark Saper (Univ. of Michigan), was generated by cloning residues 24-367 of the *E. coli* LivJ gene into the pET-29a vector (Novagen). Mutations to enable site-specific labeling (N67C and K181C), and to modify binding protein affinity (C53S and C78S), were introduced using the QuikChange site-directed mutagenesis kit (Qiagen). The resulting plasmids were verified by sequencing (GeneWiz). LIV-BP^{SS} was expressed and purified using Ni^{2+} chromatography to isolate pure LIV-BP^{SS} as previously described (32, 33). All buffers were degassed and saturated with argon to minimize intermolecular disulfide bond formation and aggregation prior to labeling.

LIV-BP^{SS} was desalted into TBS buffer (150 mM NaCl, 30 mM Tris-HCl, pH 7.0) followed by labeling with the maleimide-activated donor and acceptor fluorophores, as described previously (33). The labeled protein was purified using a Superdex 75 HiLoad 16/60 gel filtration column (GE Healthcare) in TBS buffer (150 mM NaCl, 30 mM Tris-HCl, pH 7.0). Purified, labeled LIV-BP^{SS} was flash frozen and stored in small aliquots at –80°C prior to use.

Single-molecule FRET experiments of LIV-BP^{SS} in TIRF microscope

smFRET imaging of LIV-BP^{SS} was performed using a custom-built total internal reflection fluorescence (TIRF) microscope as described above (27). Cy3-4S-DAC and other green fluorophores (Cy3 parent and Cy3B) were excited using a 532 nm laser (Laser Quantum). For time resolution titrations, the illumination intensities were 0.09 and 0.27 kW/cm^2 for 100 and 15 ms imaging, respectively; 0.55 kW/cm^2 for both 5 and 3 ms imaging; 4.06 kW/cm^2 for 1 ms imaging; and 5.46 kW/cm^2 for 0.5, 0.25 and 0.1 ms imaging. The comparative performance evaluation of smFRET pairs (Cy3-4S-DAC and Cy5-4S-AC, Cy3 parent and Cy5 parent, and Cy3B and ATTO647N) attached to LIV-BP^{SS} at 100 ms time resolution was carried out using 35 W/cm^2 illumination intensity (green laser). The fluorescence from the green and red dyes was

separated using a MultiCam LS device (Cairn) with a T635lpxr dichoric (Chroma) and projected onto two Flash 4.0 v2 sCMOS cameras (Hamamatsu).

Microfluidic imaging chambers passivated with a mixture of PEG and biotin-PEG were incubated for 5 min each with 0.8 μM streptavidin (Invitrogen) and 10 nM biotin-*tris*-NTA-Ni^{2+} (34, 35). His-tagged LIV-BP^{SS} was surface immobilized *via* the His-tag:Ni^{2+} interaction for 2 minutes. Time resolution titrations were performed in the presence of 4.5 μM leucine, which corresponds to the K_D of leucine binding to LIV-BP^{SS}. TBS buffer (150 mM NaCl, 30 mM Tris-HCl, pH 7.0) was used for all the experiments. Traces for the time resolution titrations were selected for analysis if they had single-step photobleaching, FRET above baseline >45 frames, signal-to-background noise ratio >8, number of donor blinking of events <4, background noise <70. FRET efficiency traces were idealized using SKM and a three-state model with starting FRET values of 0, 0.38, and 0.69. Apparent transition rates were calculated as the total number of observed transitions between non-zero FRET states divided by the total time in these states across all traces. For the performance evaluation of multiple FRET pairs (Cy3-4S-DAC and Cy5-4S-AC, Cy3 parent and Cy5 parent, and Cy3B and ATTO647N) attached to LIV-BP^{SS} at 100 ms time resolution, traces were selected for analysis if they had single-step photobleaching, FRET above baseline >15 frames, signal-to-background noise ratio >8, number of donor blinking of events <4, background noise <70.

Single-molecule FRET confocal spectroscopy

Single-molecule FRET measurements were performed using a MicroTime 200 equipped with a HydraHarp 400 counting module (PicoQuant). The donor and acceptor dyes were alternatively excited with a pulsed interleaved excitation scheme (36) with light from a 531 nm (LDH-P-FA-530L, PicoQuant) and a 639 nm (D-C-640, PicoQuant) diode laser, each operated at 20 MHz frequency, with an average power of 20 and 10μW at the sample, respectively. Emitted photons

were collected by the microscope objective (Olympus UPlanSApo 60x/1.20 W), focused onto a 100-μm pinhole, and then separated into four channels with a polarizing beam splitter and two dichroic mirrors (T635lpxr, Chroma). Emission was additionally filtered by bandpass filters (ET585/65M and H690/70, Chroma) before being focused onto one of four single-photon avalanche detectors (Excelitas SPCM-AQRH-TR).

FRET efficiency histograms of doubly labelled LIV-BP^{SS} were acquired on samples with a concentration of labelled protein of 60 pM in the presence of 5 μM leucine (corresponding to its binding ~K_D), and 0.01% Tween 20 (Pierce) to minimize surface adhesion (37). The data were collected for 22 hrs. To ensure consistency with TIRF experiments, confocal FRET experiments were carried out in the same microfluidic channels used for wide-field TIRF measurements.

Single-molecule FRET confocal data analysis

Consecutive photons detected in either of the donor or acceptor channels were binned with variable time intervals between 0.5 μs and 5 ms and only bins with more than 80 photons were selected for analysis. Transfer efficiencies were obtained from $E = n_A/(n_A + n_D)$, in which n_D and n_A are the numbers of donor and acceptor photons, respectively, in each burst, corrected for background, channel crosstalk, acceptor direct excitation, differences in quantum yields of the dyes and detection efficiencies (37).

To estimate the burst duration, consequent photons detected in either channel and separated by less than 100 μs were combined into one burst (38). The resulting average burst duration with a size threshold of 80 photons was ~1.7 ms. Given a photon burst recorded at time t, the probability that subsequent bursts detected after a delay time τ come from the same molecule re-entering the confocal volume is the so-called $p_{same}(\tau)$ value (39). p_{same} is 88% and 82% for the given experimental conditions and bin times of 3 ms and 5 ms, respectively (**Fig. 4e**). This allows us to show semi-quantitatively that the FRET efficiency distributions corresponding to Liv-BP^{SS} free and

bound to leucine broaden upon approaching the timescale for the interconversion of these two populations (33).

Construction of $SNAP_f$-MOR coding plasmid and generation of stable CHO cell line

The plasmid coding for the amino-terminal SNAPfast-tagged human mu opioid receptor ($SNAP_f$-MOR) was constructed by replacing the human dopamine D2 receptor coding region of the previously described pcDNA5/FRT/TO-IRES $SNAP_f$-D2 vector (40) with the coding region of human MOR, using standard PCR and sub-cloning methods. The resulting construct was confirmed by DNA sequencing and stably integrated into T-Rex Flp-In CHO cells by Flp recombinase-mediate DNA recombination and maintained as previously described(41).

Cell labeling and sample preparation for TIRF microscopy

CHO cells expressing SNAPf-MOR were prepared and labeled with 500 nM of BG-DY549 (NEB), BG-AF647 (NEB), BG-Cy3-4S-DAC, or BG-Cy5-4S-AC using previously reported methods (41). After labeling, the cells were seeded on fibronectin-coated (0.1 µg/µL) (Sigma-Aldrich) high-index cover glass (HIGHINDEX-CG, Olympus) and incubated in FluoroBrite DMEM medium (Thermo Fisher Scientific) for 1.5 hours at 37 °C in 5% CO_2. The glass coverslips were cleaned prior to use by sonicating for 20 minutes in 10% alconox, 10 minutes in deionized water, and twice for 30 minutes in 1 M potassium hydroxide. The coverslips were subsequently sonicated for 20 minutes in deionized water, rinsed in fresh deionized water, then rinsed in 100% ethanol followed by rapid drying with filtered air. The chemically cleaned slides were cleaned for 5 minutes under argon plasma before being coated with fibronectin. Before imaging, coverslips with seeded cells were washed with 15 mL of DPBS, assembled into a microscopy chamber, and then washed with imaging buffer consisting of 20 mM HEPES, 5 mM D-glucose, 135 mM NaCl, 5 mM KCl, 0.4 mM $MgCl_2$, and 1.8 mM $CaCl_2$ at pH 7.4.

Objective-based TIRF microcopy and data analysis for cell experiments

Image sequences were collected at a time resolution of 40 ms at 23 °C in ambient oxygen conditions using a previously described objective-based TIRF microscope (41) equipped with a 100X oil-immersion objective (100 X APON HOTIRF NA 1.7, Olympus) and an Evolve 512 EMCCD. SNAPf-MOR expressing cells labeled with BG-DY549 and BG-Cy3-4S-DAC were excited by a 532-nm laser line at 74.5% full power (Torus 150 mW, laser Quantum) and those labeled with BG-AF647 and BG-Cy5-4S-AC were excited by a 640-nm laser line at 55.5% full power (100 mW, Olympus). After data acquisition, the number of detected particles in select frames was determined within a region of interest within the cell using the DoG detector function of the TrackMate software. To generate fluorescence intensity distributions of particles, the u-track software was used to determine the background-corrected fluorescence intensity of those particles detected in the second frame from tracks detected from the beginning of the movie. The background was determined after photo bleaching of the particles and subtracted from the local intensities. The resulting distributions were generated from particles detected from a total of 8 cells and were fit with a single Gaussian model.

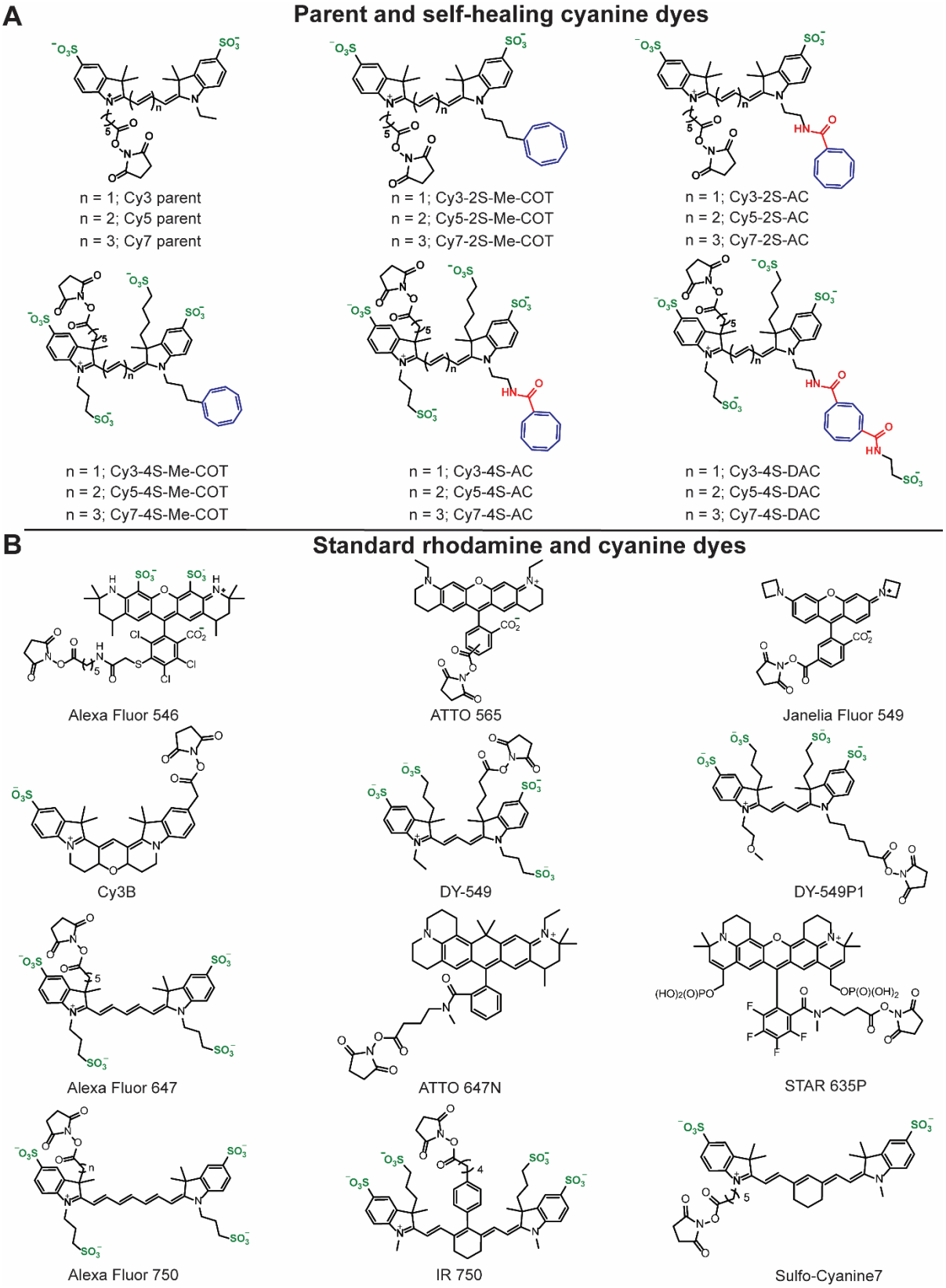

Supplementary Figure 1. Molecular structures of (*A*) parent and self-healing cyanine fluorophores, and (*B*) other cyanine and rhodamine dyes.

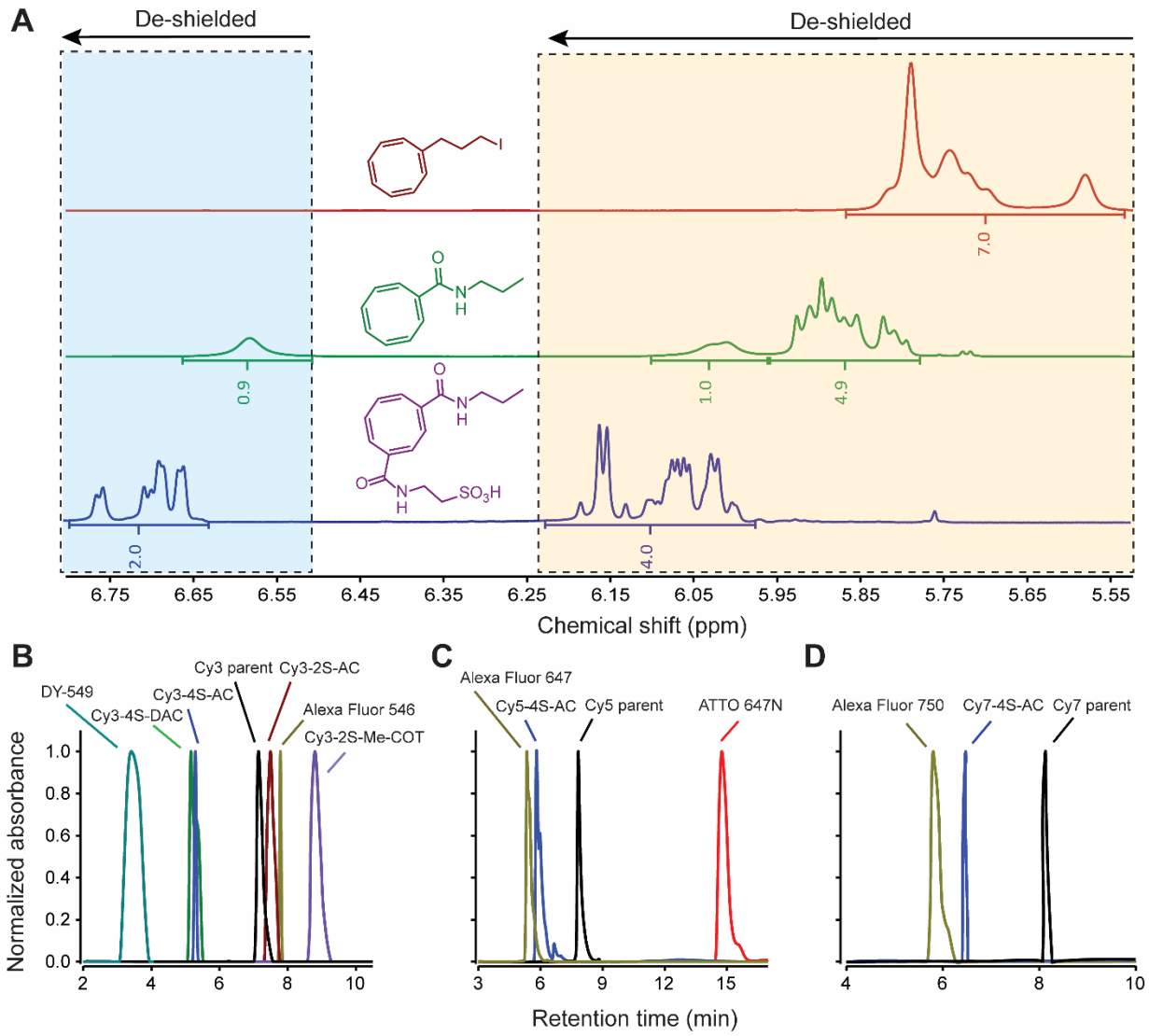

Supplementary Figure 2. ^{1}H NMR of COT molecules and retention times of parent and self-healing cyanine fluorophores and other cyanine and rhodamine dyes. (*A*) ^{1}H NMR spectra of substituted Me-COT, AC and DAC molecules in dimethyl sulfoxide-d6. Only the cyclooctatetraene ring ^{1}H signals are depicted. Left and right side dotted rectangular boxes indicate one of the cyclooctatetraene ring protons located at the *β*-position of the carbonyl group, if any, and the rest of the cyclooctatetraene ring ^{1}H's, respectively; the integrated peak area indicates the proton numbers. (*B*–*D*) Relative retention times of a set of carbo-rhodamine and cyanine dyes including self-healing derivatives.

Note: High-performance liquid chromatography evaluation of the retention times were performed using an Agilent PS325 detector, PS21X-SD1 pump modules, a Zorbax 300SB-C8 analytical column (5 µm particle, 4.6 × 150 mm) and a 10 mM triethylammonium acetate/acetonitrile linear gradient.

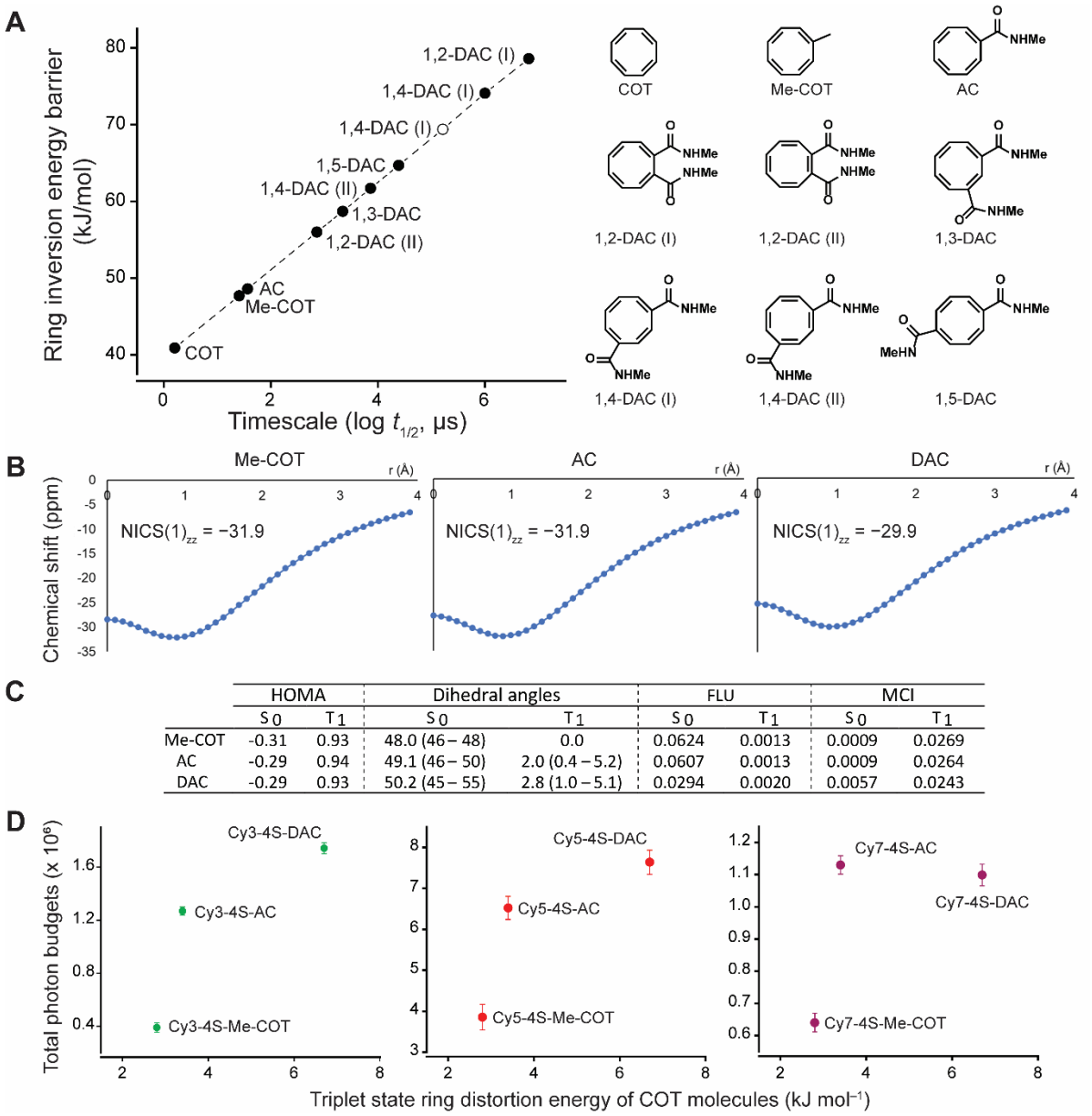

	HOMA		Dihedral angles		FLU		MCI	
	S_0	T_1	S_0	T_1	S_0	T_1	S_0	T_1
Me-COT	-0.31	0.93	48.0 (46 – 48)	0.0	0.0624	0.0013	0.0009	0.0269
AC	-0.29	0.94	49.1 (46 – 50)	2.0 (0.4 – 5.2)	0.0607	0.0013	0.0009	0.0264
DAC	-0.29	0.93	50.2 (45 – 55)	2.8 (1.0 – 5.1)	0.0294	0.0020	0.0057	0.0243

Supplementary Figure 3. Ring inversion rates, aromaticity indicators and impact of triplet state COT ring strain on self-healing fluorophore photostability. (*A*) Timescales of COT ring inversion with varying ring inversion barrier energy. All energies were calculated using OLYP-D3/6-311+G(d,p)// OLYP-D3/6-31+G(d) level except the open circle, for which CASPT2/ANO-RCC-VDZP// OLYP-D3/6-31+G(d) level was used (see **Supplementary Methods**). $t_{1/2}$ is the reaction half-life. Molecular structures of COT molecules are depicted (right side). (*B*) Nucleus-independent chemical shifts (NICS) based on aromaticity indicator of COT molecules in their T_1 states. NICS scan is used to quantify the diatropicity/paratropicity, which is calculated throughout at different positions going from the centre of the ring up to 4Å perpendicularly out-of-plane. The scans show a high pronounced minimum with negative NICS values revealing the presence of aromatic character in the T_1 state. (*C*) Harmonic oscillator model of aromaticity (HOMA), dihedral angles, aromatic fluctuation index (FLU), and multicenter index (MCI) values of COT molecules. MCI is expressed in electrons. Dihedral angles are expressed in degrees. M062X/6-31+G(d) level of theory was used (see **Supplementary Methods**). S_0 and T_1 indicate singlet ground and triplet state, respectively. (*D*) Correlations of fluorophore photostability with triplet state ring distortion energy of COT molecules. Error bars are standard deviations of six movies from at least two independent experiments in deoxygenated buffers. All calculations were performed on methylated derivatives of COT molecules to recapitulate the context when they are intramolecularly linked to fluorophores. **Note:** Me-COT, AC and DAC are strongly puckered in the S_0 state with average C-C-C-C dihedral angles of 48.0° (COT), 49.1° (AC) and 50.2° (DAC), indicating non-aromatic character.

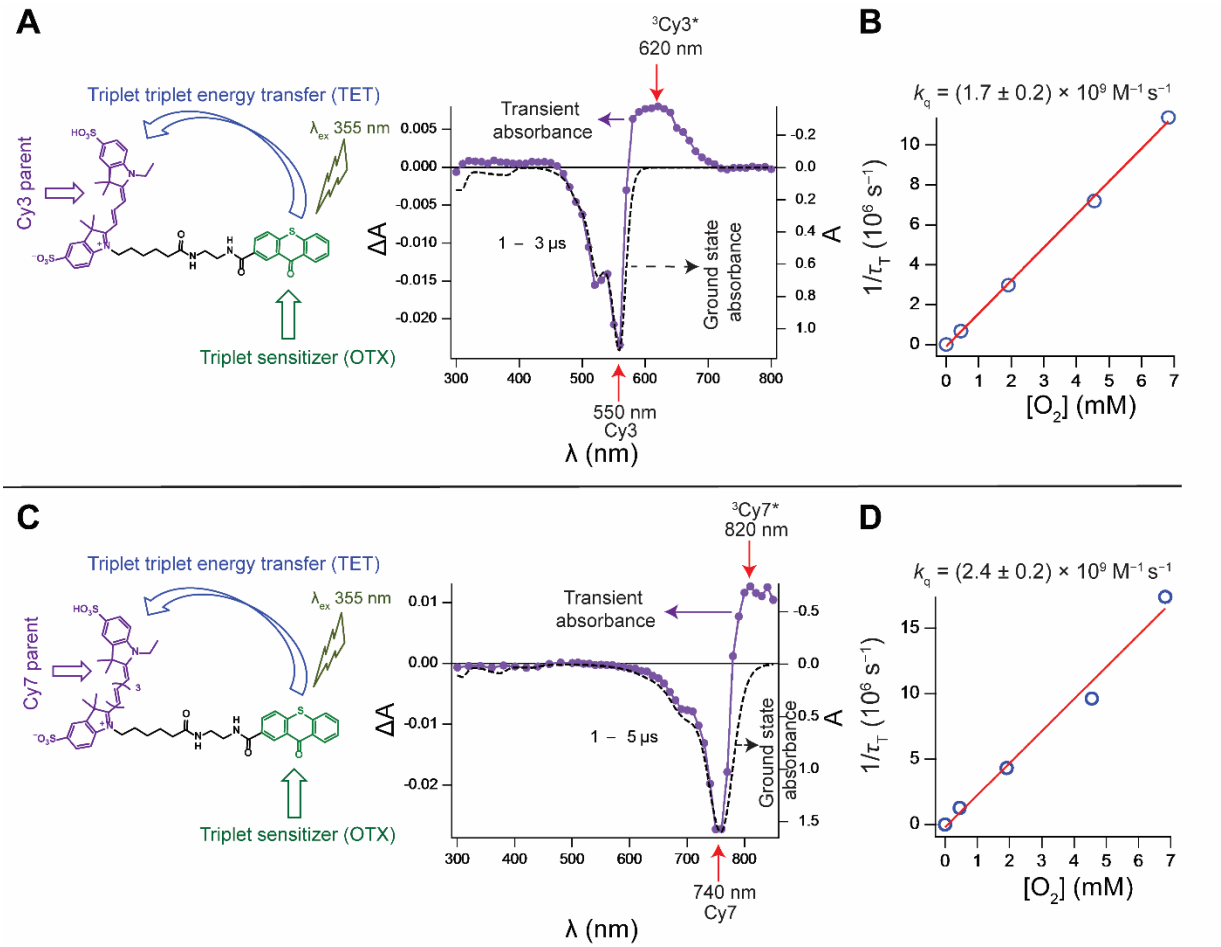

Supplementary Figure 4. Transient absorbance measurements of parent and self-healing cyanine fluorophores. (*A*, *C*) Schematics for transient absorbance measurement strategy and the experimental data of transient absorbance (left axis) and ground state absorbance (right axis) for OTX-conjugated Cy3 and Cy7 parent dyes (see **Supplementary Methods**). (*B*, *D*) Triplet state quenching of the OTX-conjugated Cy3 and Cy7 parent dyes by molecular oxygen. A, ΔA, λ, τ_T and k_q represent absorbance, change in absorbance, wavelength, triplet state lifetime and bimolecular quenching constant, respectively.

Notes:

1. The triplet state lifetime (τ_T) values of all OTX conjugated self-healing Cy3 derivatives were measured in a similar way (**Supplementary Fig. 4*A***), monitoring either the triplet decay or ground state bleaching kinetics at 620 and 550 nm, respectively.

2. The triplet state lifetime (τ_T) values of all OTX conjugated self-healing Cy7 derivatives were measured in a similar way (**Supplementary Fig. 4*C***), monitoring either the triplet decay or ground state bleaching kinetics at 820 and 740 nm, respectively.

3. The transient absorption spectra of Cy5 parent dye can be found in our earlier work (41). Consistent with the earlier observations that the triplet transient and ground state bleaching of Cy5 parent dye appear at 700 and 645 nm, respectively, we measured here the triplet state lifetime (τ_T) values of OTX conjugated Cy5-4S-Me-COT, Cy5-4S-AC and Cy5-4S-DAC derivatives. The τ_T values of Cy5 parent, Cy5-2S-Me-COT and Cy5-2S-AC derivatives were taken from our previous study (41).

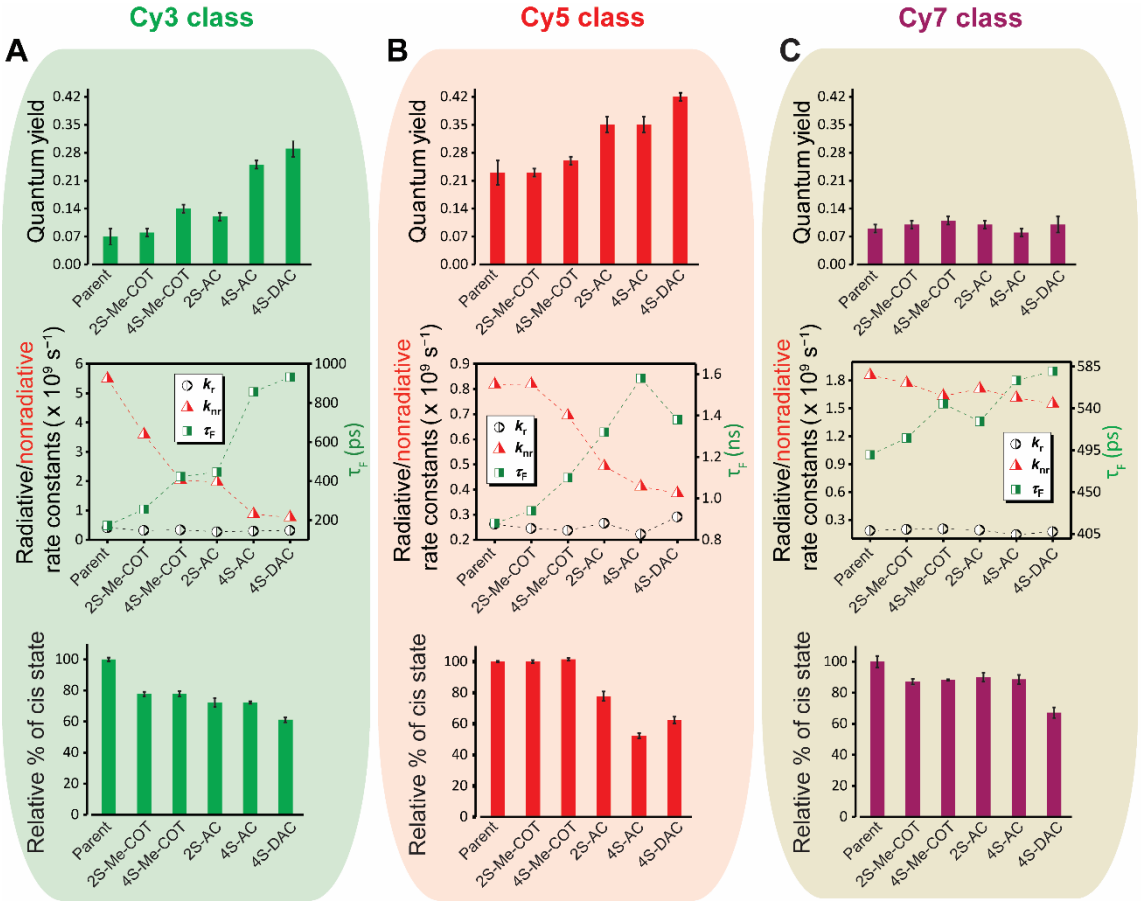

Supplementary Figure 5. Fluorescence quantum yield, fluorescence lifetime, radiative and nonradiative rate constants, and cis state population of parent and self-healing cyanine fluorophores. (*A*–*C*) Evaluation of fluorescence quantum yield (Φ_F), fluorescence lifetime (τ_F), radiative (k_r) and nonradiative (k_{nr}) rate constants, and relative population of cis state of (*A*) Cy3, (*B*) Cy5 and (*C*) Cy7 classes of fluorophores. Fluorescence quantum yield and fluorescence lifetime measurements were carried out with free cyanine dyes (see **Supplementary Methods**), whereas cis state populations were measured using cyanine dyes bound to DNA oligonucleotides in ambient conditions (see **Supplementary Methods**). Error bars are standard deviations of data from at least three independent experiments.

Note: k_r and k_{nr} values were calculated from the experimental fluorescence quantum yield (Φ_F) and fluorescence lifetime (τ_F) values using the following equations (42).

$k_r = \Phi_F/\tau_F$ and $k_{nr} = (1 - \Phi_F)/\tau_F$

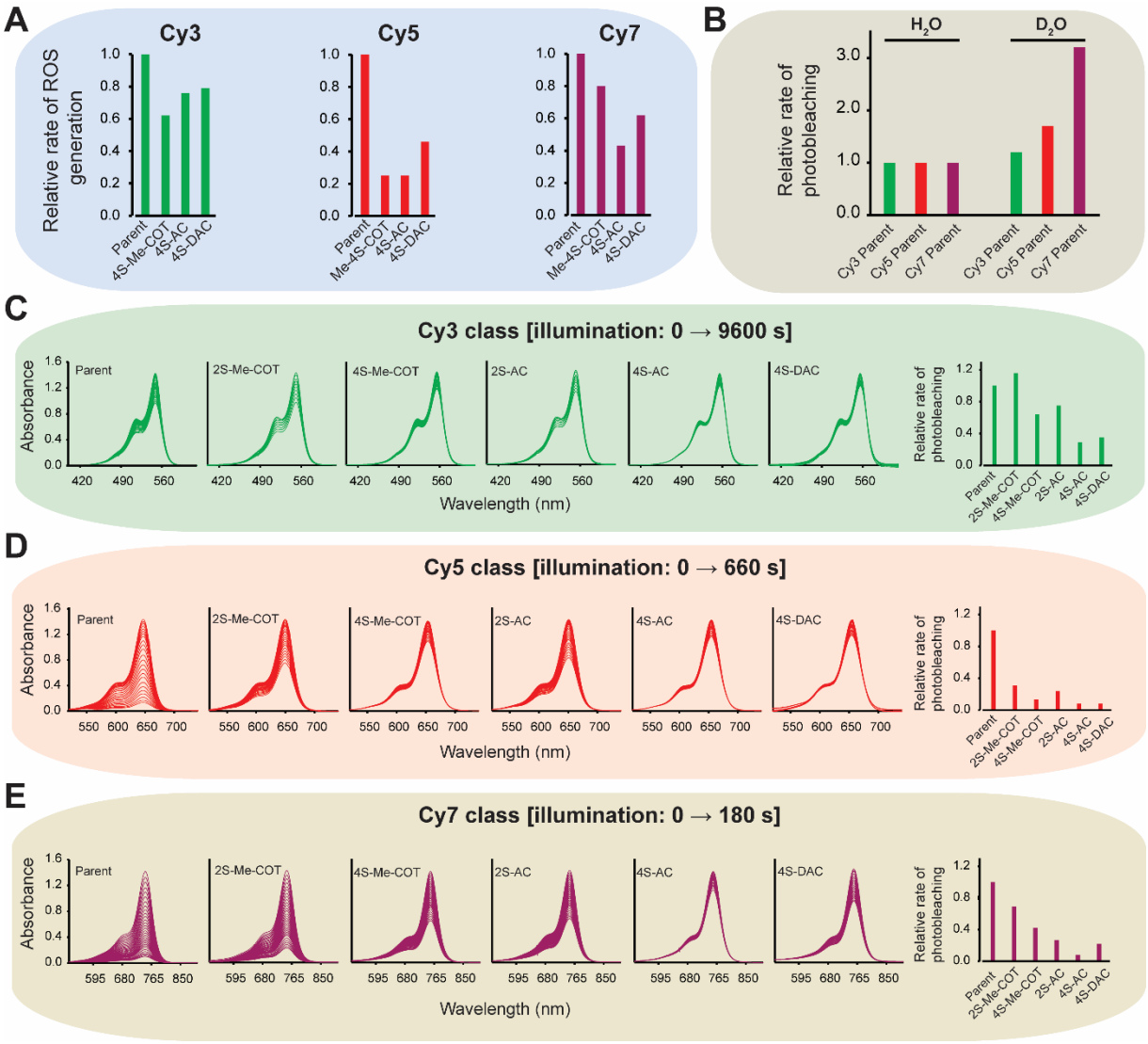

Supplementary Figure 6. Reactive oxygen species generation and bulk photostability of parent and self-healing cyanine fluorophores. (*A*) Relative rates of reactive oxygen species (ROS) generation in water (see **Supplementary Methods**). (*B*) Photobleaching rates of parent cyanine fluorophores in D_2O relative to their individual photobleaching rates in H_2O. As lifetime of singlet oxygen is 20-fold longer in D_2O than H_2O (42), the photobleaching rates are higher in D_2O. (*C*–*E*) Bulk photostability of Cy3, Cy5 and Cy7 classes of fluorophores (see **Supplementary Methods**). Measurements were carried out with free dyes (not bound to biomolecules) in water at room temperature in the presence of oxygen.

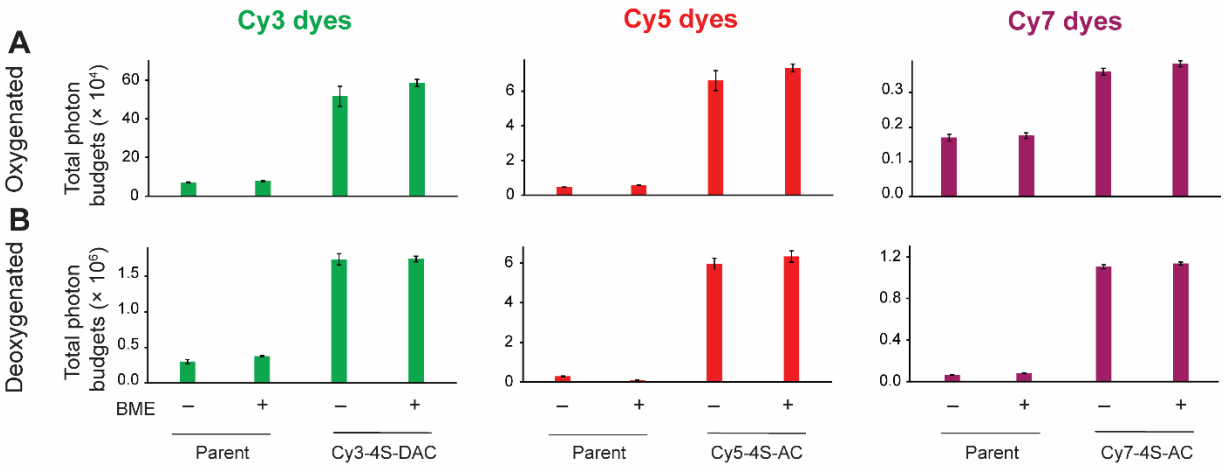

Supplementary Figure 7. Impact of BME on the photostability of parent and self-healing cyanine fluorophores. Photostability of parent cyanine dyes and self-healing fluorophores bound to DNA oligonucleotides in the presence and absence of BME (see **Supplementary Methods**) in (*A*) oxygenated and (*B*) deoxygenated imaging buffers. Error bars are standard deviations of four movies from two independent experiments.

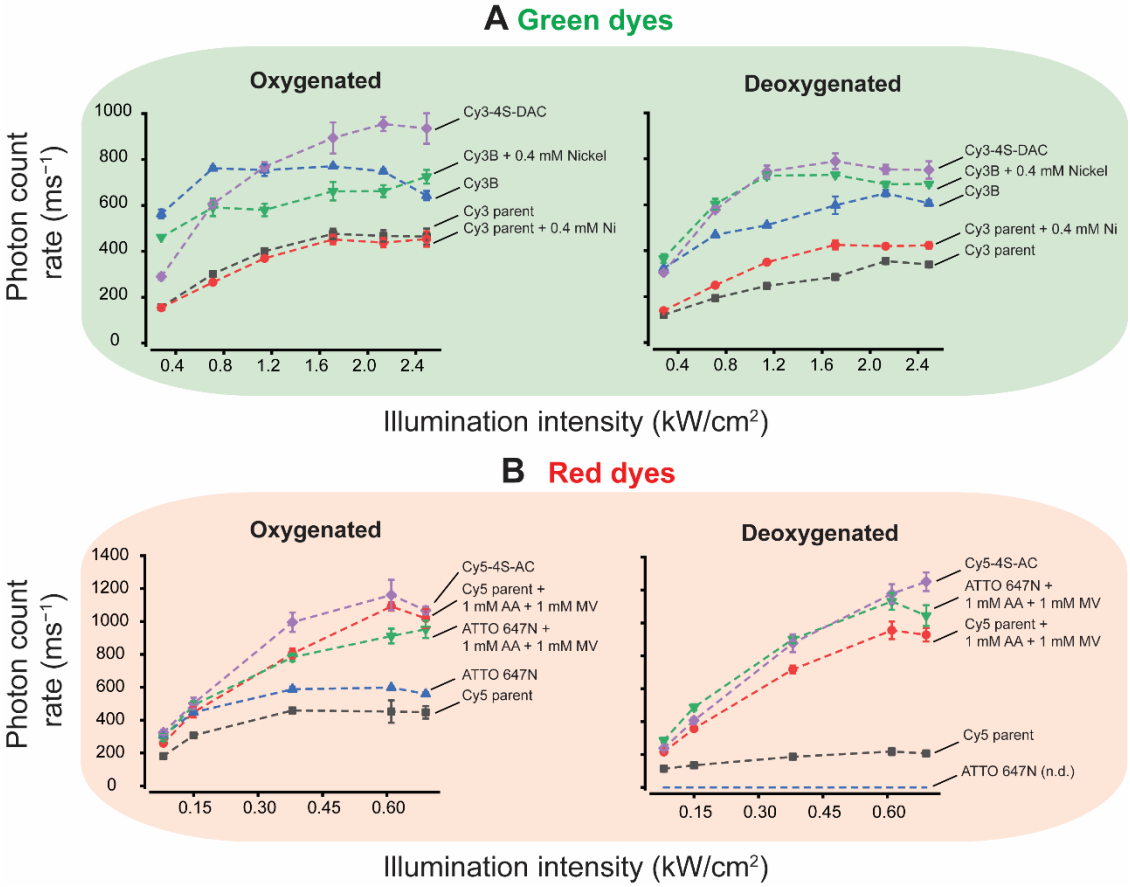

Supplementary Figure 8. Photon count rates at high time resolution (1 ms) for parent and self-healing cyanine fluorophores as well as other cyanine and rhodamine dyes. (*A*) Comparisons of photon count rates of self-healing Cy3 (Cy3-4S-DAC), Cy3B, parent Cy3 and (*B*) self-healing Cy5 (Cy5-4S-AC), ATTO 647N and parent Cy5 dyes bound to DNA oligonucleotides in the presence and absence of oxygen at 1 ms time resolution. Parent Cy3 and Cy5, Cy3B and ATTO 647N were also interrogated in the presence of solution additives. Error bars are standard deviations of at least two technical replicates. AA and MV stand for ascorbic acid and methyl viologen, respectively. 'n.d.' implies not determinable.

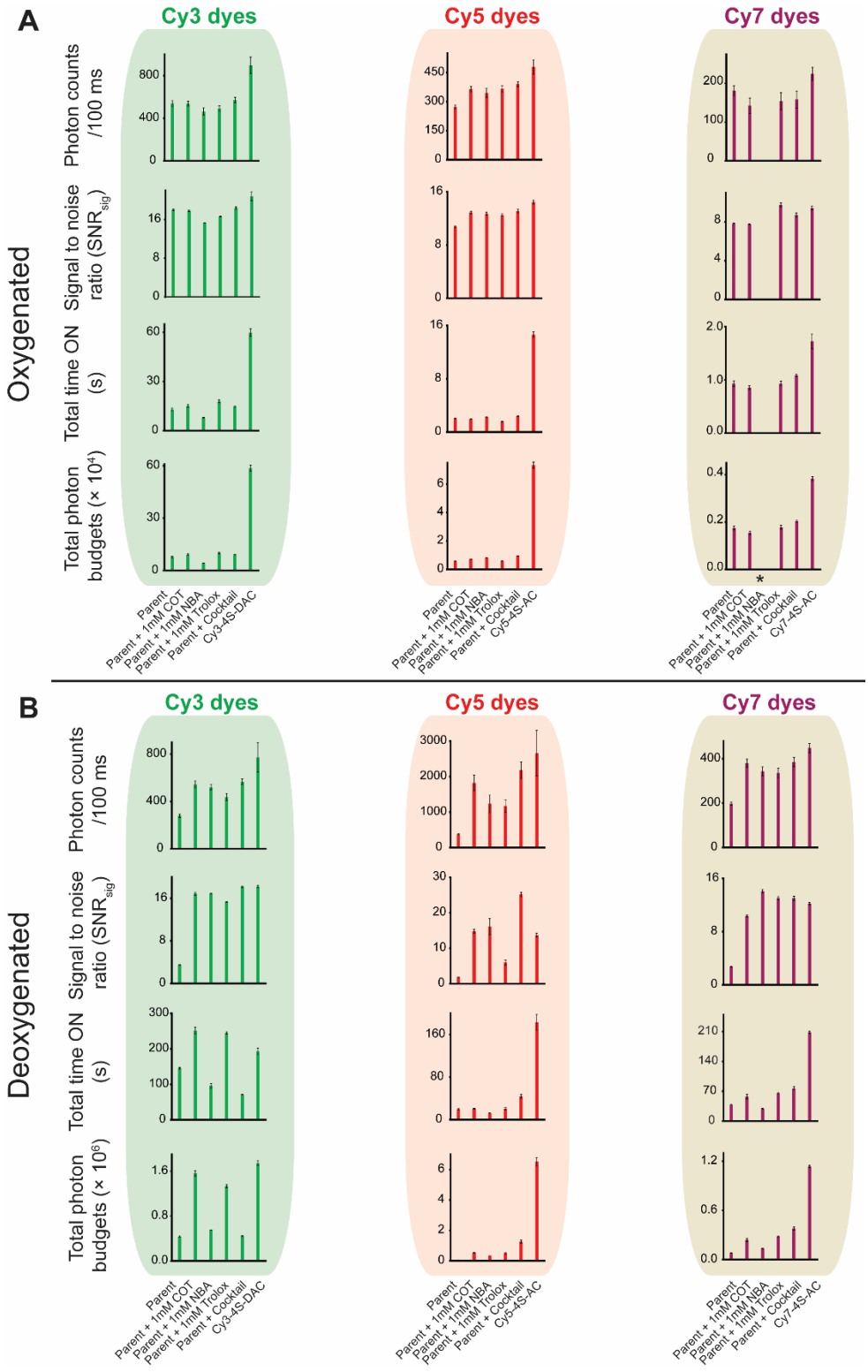

Supplementary Figure 9. Photophysical evaluation of parent cyanine fluorophores in the absence and presence of solution additives and self-healing cyanine fluorophores (no additive). (*A*, *B*) Comparisons of photophysical properties of DNA oligonucleotides bound parent cyanines in the absence and presence of solution additives and the best performing self-healing cyanine dyes in (*A*) oxygenated and (*B*) deoxygenated imaging buffers. 'Cocktail' refers to a mixture of 1 mM COT, 1 mM NBA and 1 mM Trolox. Error bars are standard deviations of six movies from at least two independent experiments. (*) indicates data that were not quantified due to low brightness and fast photobleaching.

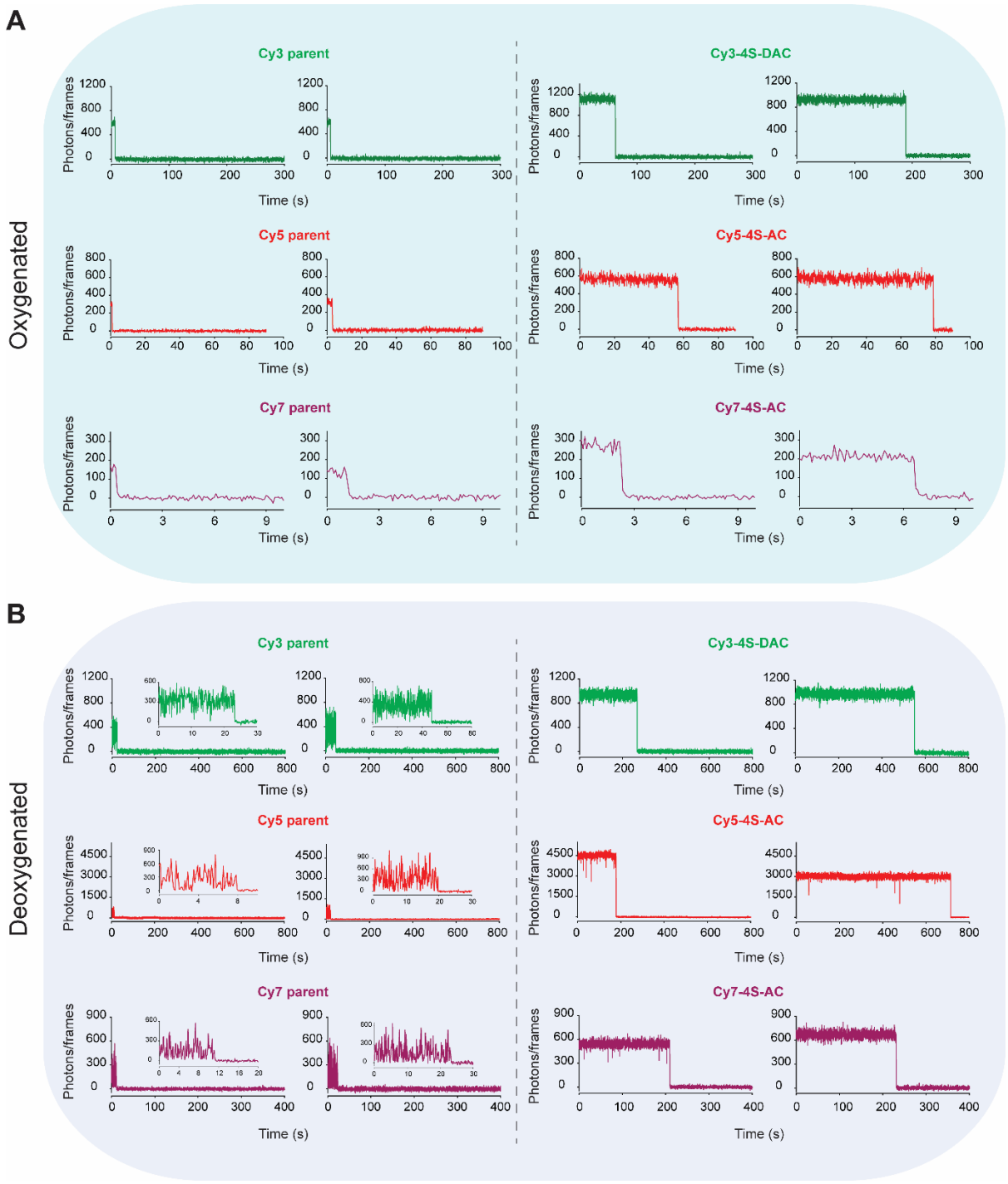

Supplementary Figure 10. Blinking characterization of parent and self-healing cyanine fluorophores. Representative single-molecule fluorescence traces of parent and self-healing cyanine fluorophores bound to DNA oligonucleotides in (*A*) oxygenated and (*B*) deoxygenated imaging buffers at 100 ms time resolution.

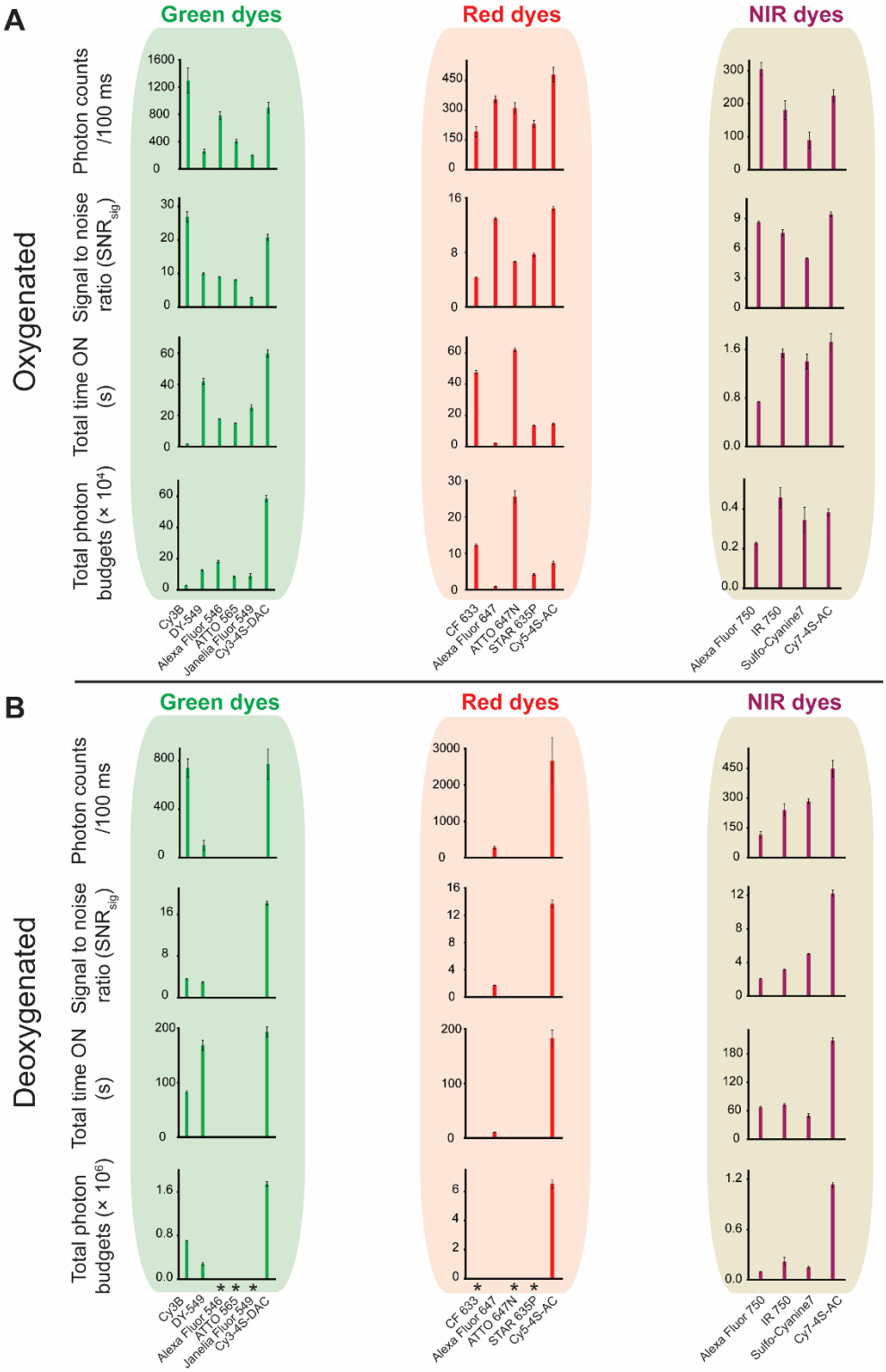

Supplementary Figure 11. Comparative photophysical evaluation of self-healing fluorophores and other cyanine and rhodamine dyes in the absence of solution additives. (*A*, *B*) Comparisons of photophysical properties of self-healing cyanine fluorophores and other cyanine and rhodamine dyes bound to DNA oligonucleotides in (*A*) oxygenated and (*B*) deoxygenated imaging buffers. Error bars are standard deviations of six movies from at least two independent experiments. (*) indicates systems that were not quantified due to low brightness and fast photobleaching.

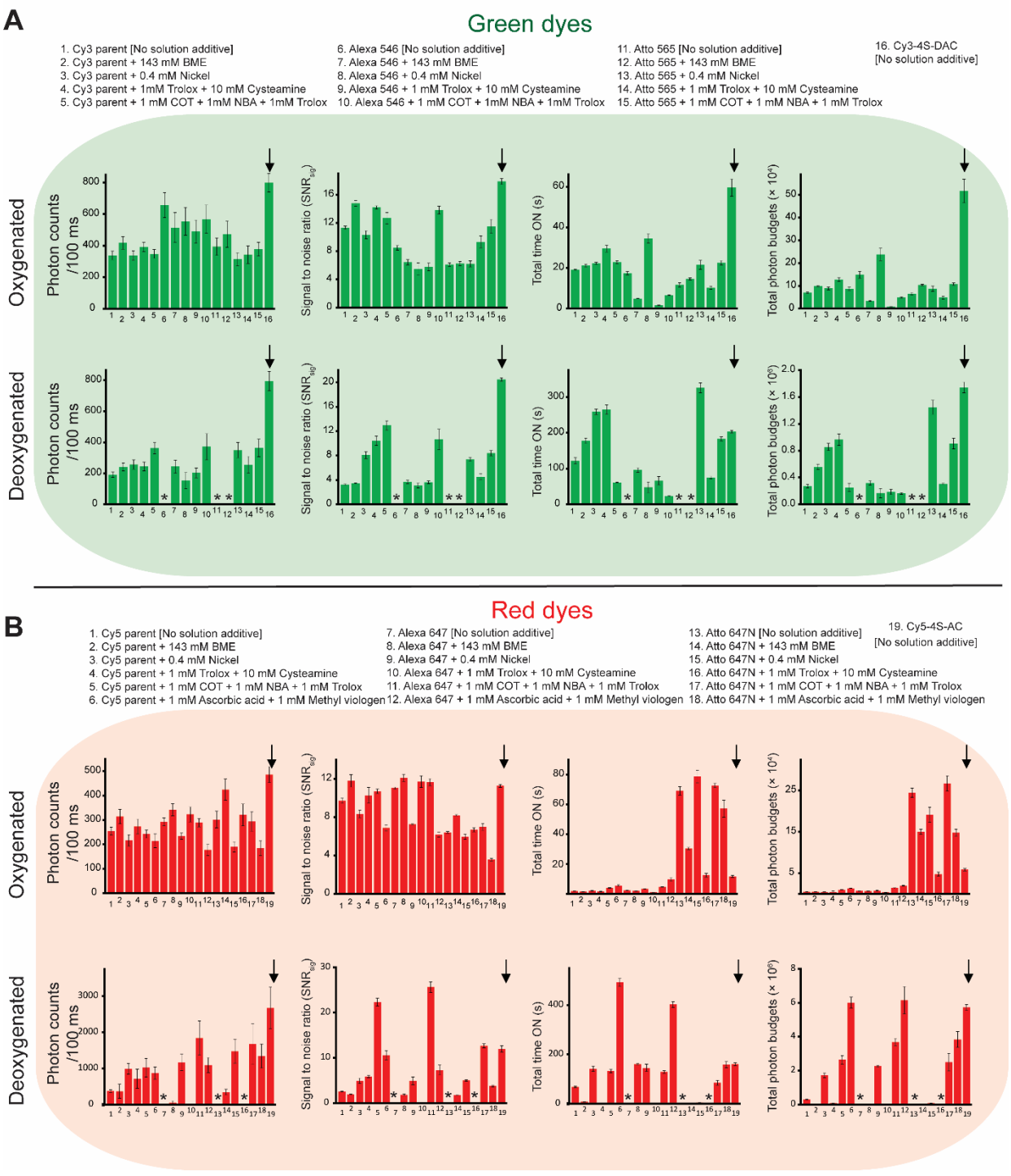

Supplementary Figure 12. Comparative photophysical evaluation of self-healing fluorophores (no additive) and other cyanine and rhodamine dyes in the absence and presence of solution additives with no supplementary BME. (*A*, *B*) Comparisons of photophysical properties of (*A*) green and (*B*) red dyes with the best-performing self-healing dyes bound to DNA oligonucleotides in oxygenated and deoxygenated imaging buffers. Error bars are the standard deviation of four movies from two independent experiments. (*) indicates systems that were not quantified due to low brightness and fast photobleaching. Downward arrows indicate self-healing fluorophores.

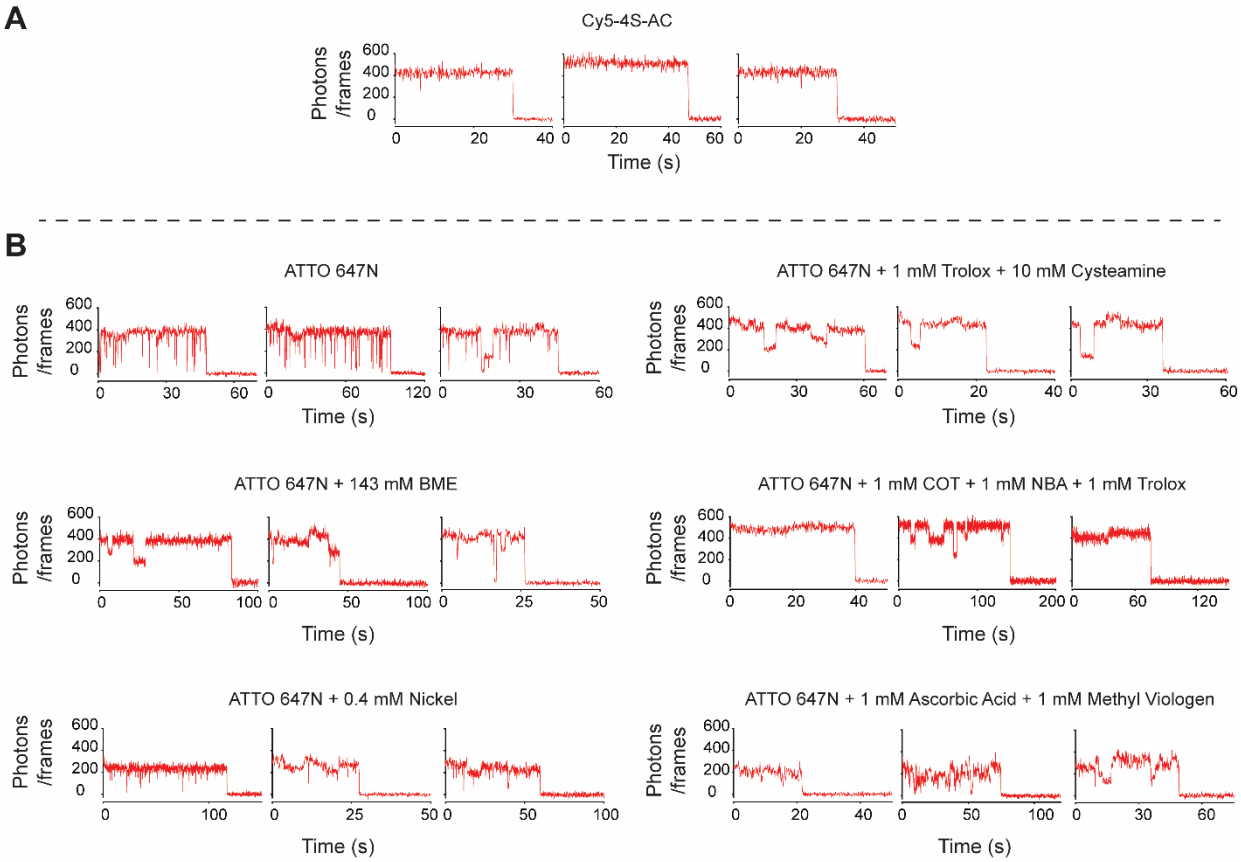

Supplementary Figure 13. Comparison of single-molecule fluorescence traces of self-healing cyanine and rhodamine dyes. Representative single-molecule fluorescence traces of (*A*) Cy5-4S-AC and (*B*) ATTO 647N dyes bound to DNA oligonucleotides in oxygenated buffers in the absence of supplementary BME at 100 ms time resolution.

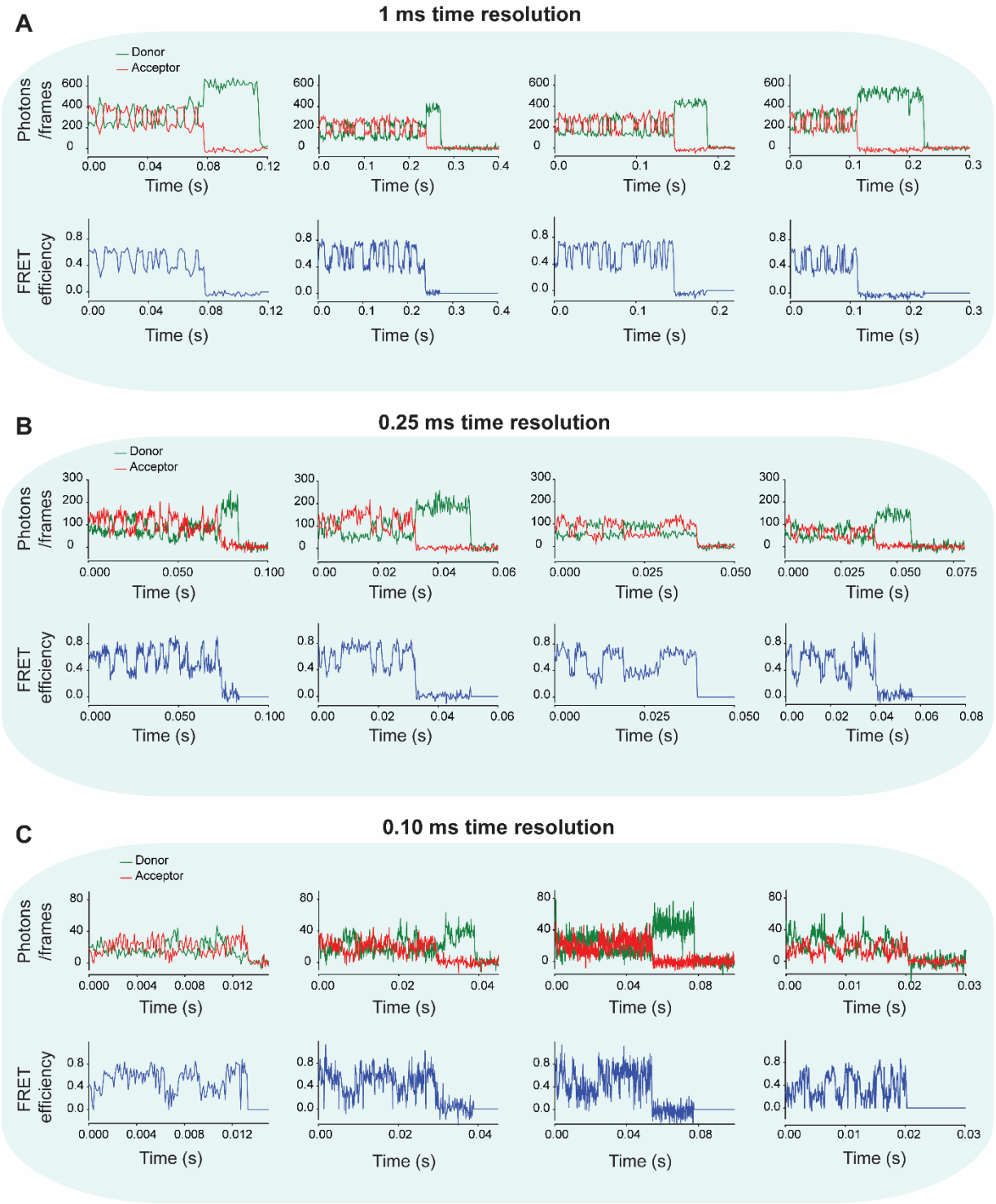

Supplementary Figure 14. smFRET experiments of self-healing cyanine fluorophores labeled LIV-BP^{SS}. (*A–C*) Representative single-molecule fluorescence traces and smFRET trajectories of Cy3-4S-DAC and Cy5-4S-AC labeled LIV-BP^{SS} using wide-field illumination and camera-based detection strategies at (*A*) 1 ms, (*B*) 0.25 ms and (*C*) 0.10 ms time resolution in the presence of leucine (corresponding to K_D) in oxygenated buffers. The illumination intensity was 4.06 kW/cm^2 for 1 ms imaging. The illumination intensity was same for both 0.25 and 0.10 ms imaging (5.46 kW/cm^2).

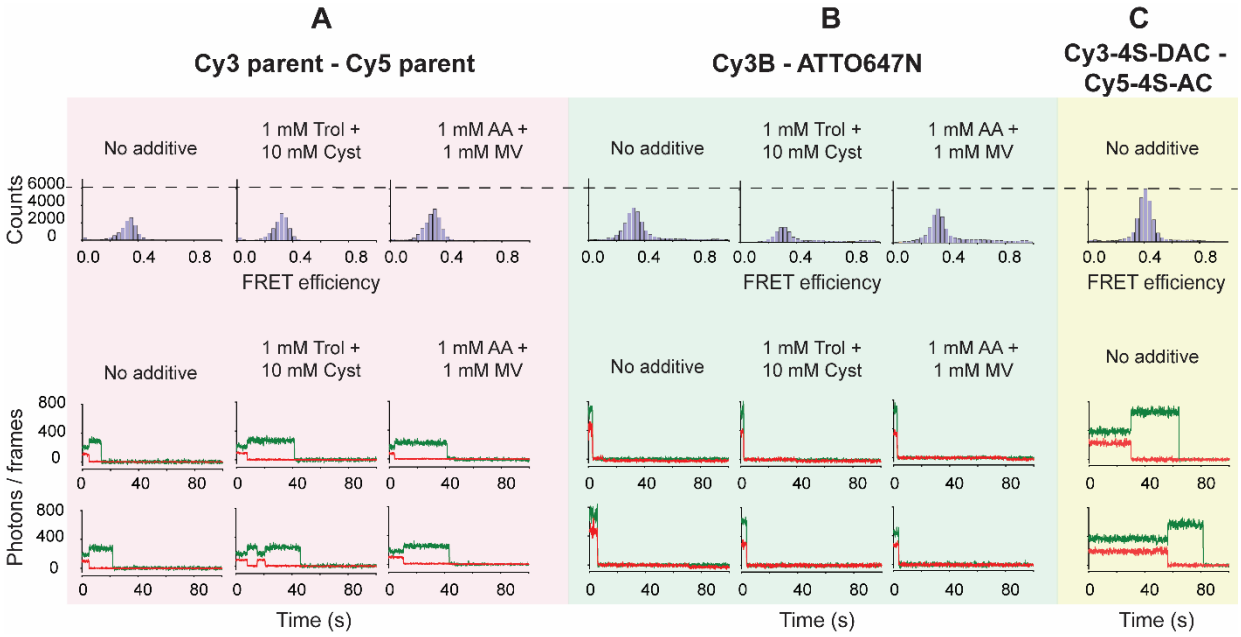

Supplementary Figure 15. Comparisons of smFRET experiments of self-healing cyanine fluorophores and other cyanine and rhodamine dyes labeled LIV-BP^{SS}. Cumulative population histograms and representative smFRET trajectories of surface immobilized LIV-BP^{SS} labeled with (*A*) Cy3 parent and Cy5 parent dye pair, (*B*) Cy3B and ATTO647N dye pair, and (*C*) Cy3-4S-DAC and Cy5-4S-AC dye pair at 100 ms time resolution in oxygenated buffers in the absence of leucine. Trol, Cyst, AA and MV represent Trolox, cysteamine, ascorbic acid and methyl viologen, respectively.

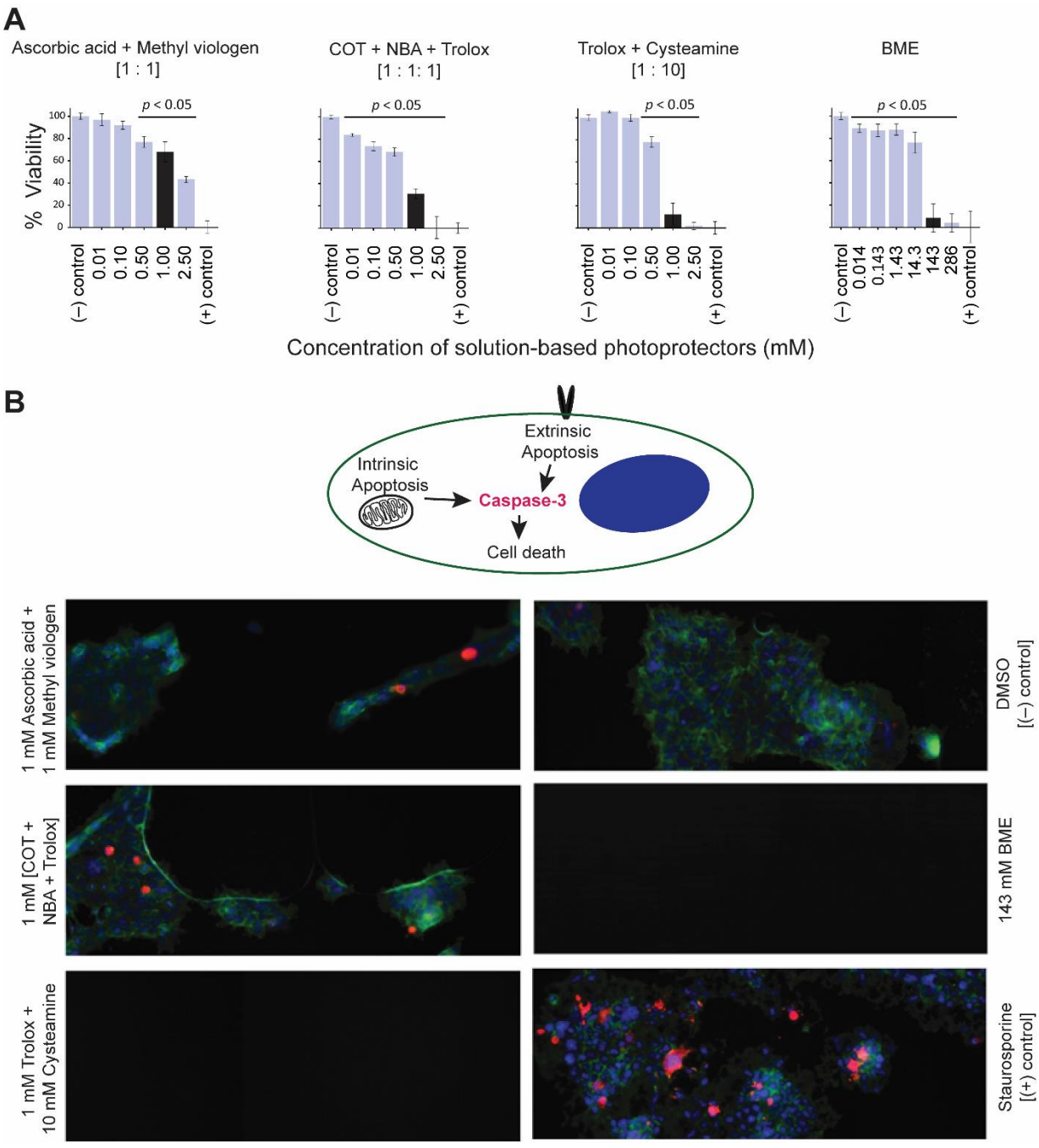

Supplementary Figure 16. Assessments of cytotoxicity with commonly used photoprotective agents for biological imaging. (*A*) Promega CellTiter-Glo® Luminescent assay performed on HEK293H cells treated for 2 hrs with various concentrations of photoprotective agents used in biological imaging (see **Supplementary Methods**). Black bars indicate commonly used working concentrations. The *p* values (statistical significance levels) are reported with respect to a (–) control. Error bars are standard errors from six technical replicates. (*B*) Immunofluoresence images of HEK293H cells treated with commonly used concentrations of photoprotective agents as in (*A*) (see **Supplementary Methods**). DAPI (blue), Phalloidin (green), and cleaved Caspase-3 (red) highlight nuclei, cytoskeleton, and apoptotic cell death (schematic), respectively.

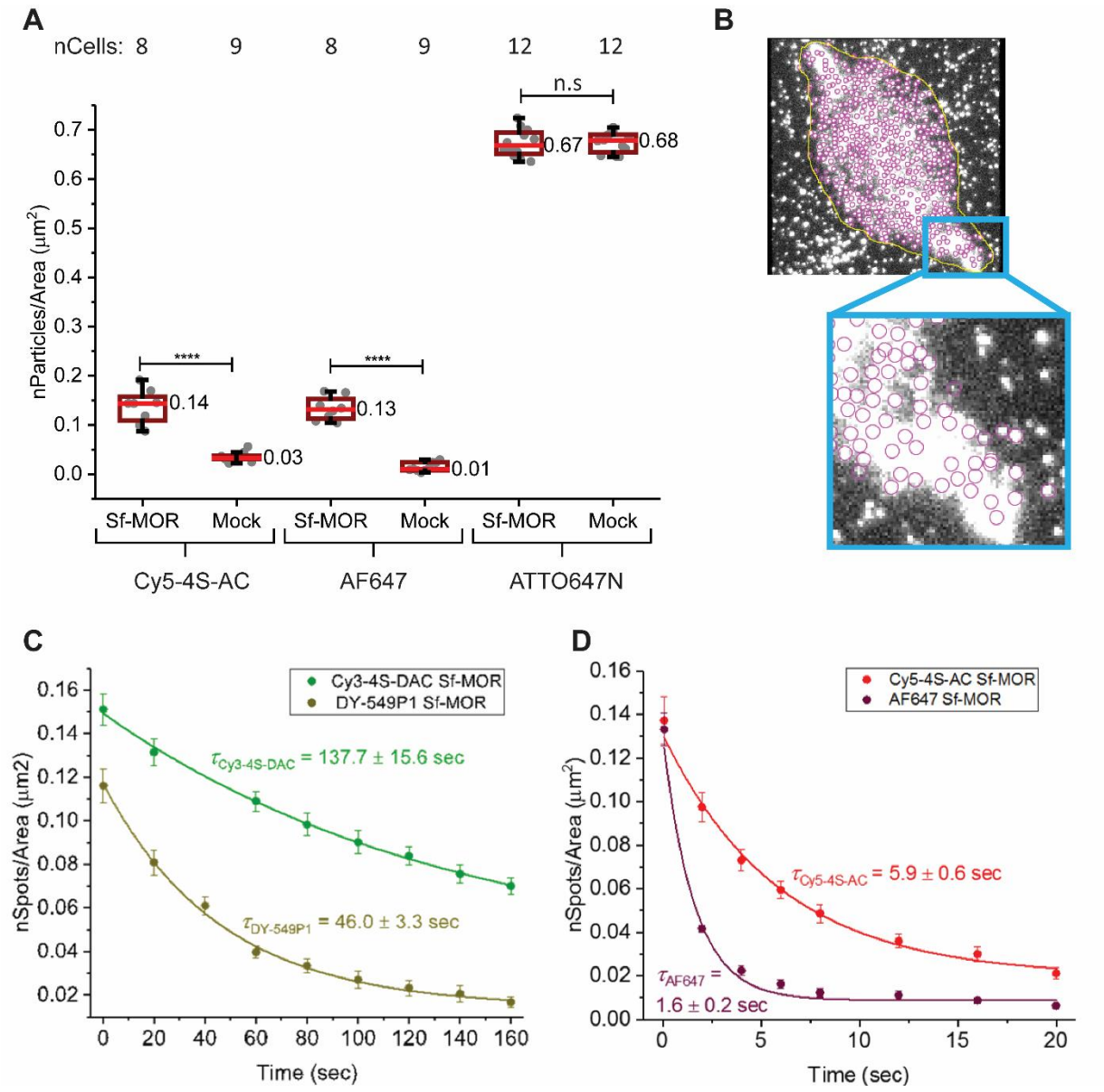

Supplementary Figure 17. Evaluations of non-specificity and photobleaching times of self-healing cyanine fluorophores and other cyanine and rhodamine dyes in living-cells. (*A*) Distribution of particle densities for CHO cells expressing $SNAP_f$ (Sf)-MOR and Mock CHO cells labeled with 500 nM Cy5-4S-AC-BG, AF647-BG, or ATTO647N-BG. Dots depict the number of particles per area for each cell. Box plots indicate the median (central line, value shown) and interquartile range (lower and upper lines of box representing the 25- and 75-percentiles, respectively) while the whiskers represent points that fall within 1.5 times the interquartile range. A *t*-test was performed to obtain *p*-values (****$p < 0.0001$; n.s. = 0.8968). (*B*) Representative Mock CHO cell labeled with ATTO647N-BG. Spot detection under-represents the number of particles due to unresolved spots. (*C*, *D*) Photobleaching times shown as a function of the number of spots (nSpots) per cell area over time for (*C*) Cy3-4S-DAC and DY-549P1 labeled $SNAP_f$-MOR (Sf-MOR) and (*D*) Cy5-4S-AC and AF647 labeled Sf-MOR expressed in CHO cells at ambient oxygen conditions. Each curve includes the nSpot/area from 8 different cells. The error bars are the standard error of the mean for each point.

Supplementary Table 1. [see next page]: Triplet energies (E_T), inversion barriers (ΔE_{inv}), energy difference between the optimal triplet state and the planar singlet state ($\Delta E_{TS(S0)\rightarrow T1ad}$), energy for vertical excitation from the planar singlet (D_{4h}) to the triplet state ($\Delta E_{TS(S0)\rightarrow T1vert}$), vertical emission energy from the optimal triplet state structure to the singlet state ($\Delta E_{T1ad\rightarrow S0}$), triplet state ring distortion energy, and ground state HOMO energy of COT molecules (see **Supplementary Methods**). Electronic energies (normal), Gibbs free energies (italics) and Gibbs free energies including solvent corrections (bold) are provided at the M062X and OLYP levels. The triplet energies are computed as energy differences between the singlet ground state and the first triplet excited state at their optimal geometries including thermal corrections. All the calculations were done in gas phase except the triplet and ring inversion energies, where solvation (ethanol) corrections were included (see **Supplementary Methods**). The energy values in parentheses are for the second bond-shifted isomer of the respective COT molecules. A simplified schematic of the aforementioned various energies is displayed below.

Simplified schematic displaying the various energies listed in Supplementary Table 1 (see next page): Red arrows correspond to energies between stationary points on the S_0 and T_1 potential energy surfaces, while blue arrows correspond to energies where one of the structures is a non-stationary point in one of the two states or when an energy is calculated as a difference between two energies, where one is based on a non-stationary point.

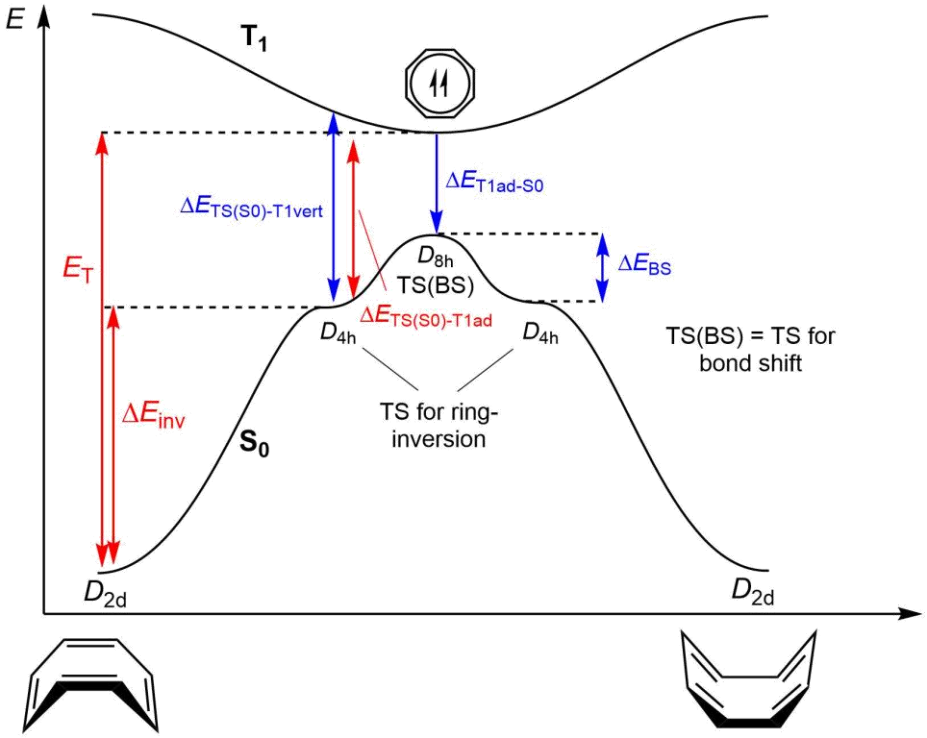

	E_T (kJ/mol)		ΔE_{inv} (kJ/mol)		$\Delta E_{TS(S0)-T1ad}$ (kJ/mol)		$\Delta E_{TS(S0)\rightarrow T1vert}$ (kJ/mol)		$\Delta E_{T1ad\rightarrow S0}$ (kJ/mol)		Ring distortion energy (kJ/mol)	HOMO (eV)	
	OLYP	M062X	OLYP	M062X	OLYP	M062X	OLYP	M062X	OLYP	M062X			
COT	47.5, *46.1*	105.7, *101.5*, **104.4**	36.4, *40.9*, **40.9**	58.9, *63.2*	11.1, *5.2*	46.8, *38.3*	21.3	79.9	–8.7	–24.0		–7.51	
Mono-substituted COT molecules		**99.3**											
		104.8											
		105.0											
		105.2											
		105.5											
		107.7											
		109.5											
		109.7											
		111.7										–7.43	
	59.0, *54.0*	116.1, *109.6*, **112.3**	42.0, *47.5*, **47.7**	63.3, *68.9*	17.0, *6.5*	52.8, *40.7*	33.7	86.4	–8.5	–23.4	2.8		
		113.4										–7.72	
	60.2, *58.0*	117.6, *114.4*, **117.2**	46.5, *50.4*, **48.6**	70.7, *76.2*	13.7, *7.6*	46.9, *38.2*	29.3	79.9	–8.2	–23.4	3.4		
Di-substituted COT molecules		**116.5**											
		120.7										–7.87	
		120.9											
	68.8, *68.4*	123.1, *119.9*, **124.2**	58.7, *66.8*, **64.7**	79.5, *86.5*	10.1, *1.6*	43.6, *33.4*	27.0	77.5	–7.6	–23.0	6.9		
	68.8, *63.3*	122.0, *120.3*, **125.4**	65.5, *66.8*, **58.7**	86.6, *93.4*	3.3, *–3.5*	35.4, *26.9*	25.9	77.5	–7.6	–22.7	5.9	–7.85	
		126.5											
	70.4, *68.1*	126.0, *125.2*, **131.6 (124.3)**	67.4, *74.4*, **74.1 (61.7)**	86.9, *96.6*	3.0, *–6.3*	39.1, *28.6*	18.5	75.7	–7.9	–22.6	6.7	–7.91 (–7.89)	
	81.5, *80.5*	135.5, *133.4*, **137.6 (115.8)**	71.2, *78.5*, **78.6 (56.0)**	89.2, *97.4*	10.3, *2.0*	46.3, *36.0*	27.7	82.9	–7.9	–23.2	9.3	–7.93 (–7.84)	
Tetra-substituted COT molecules		**150.0**											
		150.0											
		153.6											
		154.9											
		166.5											
		174.0											

Supplementary Table 2. Computed Gibbs energy (*ΔG*) of reaction of triplet state quenchers (TSQs) with molecular oxygen ($^3O_2$) [see **Supplementary Methods**; [a]SC: percentage of spin contamination in the various TSQs. SC($^3O_2$): 2% (both methods); [b] the calculation is expensive].

	ΔG (kJ/mol)			
TSQs	B3LYP	M062X	G3MP2B3	G4MP2
COT	101.99	54.47	23.87 (1% SC[a])	24.79 (1% SC)
Me-COT	100.76	47.31	19.71 (3% SC)	23.57 (5% SC)
AC	89.25	41.87	21.28 (4% SC)	28.75 (4% SC)
DAC	78.34	30.82	14.66 (4% SC)	-[b]
Anthracene	2.94	-23.75	-62.56 (8% SC)	-51.97 (7% SC)
NBA	-66.30	-90.24	-166.15 (29% SC)	-148.45 (29% SC)

Supplementary Table 3: Photophysical parameters of cyanine dyes. Steady-state absorption (λ_{abs}) and emission (λ_{em}) wavelength maxima, fluorescence quantum yield (Φ_F), fluorescence lifetime (τ_F), triplet state lifetime (τ_T) and total photon budgets of Cy3, Cy5, and Cy7 class of dyes. λ_{abs}, λ_{em}, Φ_F, τ_F were measured for free cyanine dyes (not conjugated with biomolecules) in water. τ_T was measured for OTX-conjugated cyanine dyes in acetonitrile. The error bars are standard deviations.

Dyes	λ_{abs} (nm)	λ_{em} (nm)	Φ_F	τ_F	τ_T (μs)	Total photon budgets in oxygenated buffers (× 10^4)	Total photon budgets in deoxygenated buffers (× 10^6)
Cy3 parent	550	561	0.07 ± 0.02	173 ± 4 ps	90 ± 1	11.2 ± 0.1	0.37 ± 0.01
Cy3-2S-Me-COT	551	563	0.08 ± 0.01	256 ± 3 ps	18 ± 1	13.6 ± 0.2	0.59 ± 0.01
Cy3-4S-Me-COT	555	567	0.14 ± 0.01	423 ± 2 ps	6.6 ± 0.3	14.9 ± 0.2	0.64 ± 0.02
Cy3-2S-AC	552	565	0.12 ± 0.01	447 ± 1 ps	6 ± 1	32.2 ± 0.4	1.1 ± 0.1
Cy3-4S-AC	555	567	0.25 ± 0.01	857 ± 2 ps	0.13 ± .01	40.8 ± 0.4	1.3 ± 0.1
Cy3-4S-DAC	555	568	0.29 ± 0.02	932 ± 2 ps	1.1 ± 0.1	58.2 ± 0.9	1.7 ± 0.1
Cy5 parent	647	664	0.23 ± 0.03	880 ± 5 ps	110 ± 5	0.57 ± 0.01	0.10 ± 0.01
Cy5-2S-Me-COT	649	666	0.23 ± 0.01	940 ± 5 ps	0.40 ± .02	2.1 ± 0.1	2.5 ± 0.1
Cy5-4S-Me-COT	654	671	0.26 ± 0.01	1.1 ± 0.1 ns	0.45 ± .02	2.1 ± 0.1	3.5 ± 0.1
Cy5-2S-AC	650	669	0.35 ± 0.02	1.3 ± 0.1 ns	0.08 ± .01	5.1 ± 0.1	5.2 ± 0.2
Cy5-4S-AC	654	673	0.35 ± 0.02	1.6 ± 0.1 ns	0.20 ± .01	7.3 ± 0.1	6.4 ± 0.1
Cy5-4S-DAC	655	674	0.42 ± 0.01	1.4 ± 0.1 ns	0.54± .02	5.8 ± 0.1	7.6 ± 0.1
Cy7 parent	747	773	0.09 ± 0.01	490 ± 3 ps	82± 1	0.18 ± 0.01	0.15 ± 0.10
Cy7-2S-Me-COT	750	776	0.10 ± 0.01	508 ± 3 ps	8 ± 2	0.21 ± 0.01	0.57 ± 0.01
Cy7-4S-Me-COT	755	781	0.11 ± 0.01	545 ± 2 ps	8.8 ± 0.3	0.35 ± 0.01	0.64 ± 0.01
Cy7-2S-AC	751	777	0.10 ± 0.01	526 ± 2 ps	2.5 ± 0.1	0.30 ± 0.01	1.1 ± 0.1
Cy7-4S-AC	754	780	0.08 ± 0.01	570 ± 2 ps	2.4 ± 0.1	0.38 ± 0.01	1.1 ± 0.1
Cy7-4S-DAC	755	780	0.10 ± 0.02	580 ± 2 ps	24 ± 2	0.31 ± 0.01	1.1 ± 0.1

Supplementary Information for Synthesis

Synthesis and Characterization

General Procedures

Unless otherwise stated, all commercially available materials were purchased from Aldrich, TCI, or Alfa Aesar and were used without any further purification. When necessary, solvents and reagents were dried prior to use, using standard protocols. All non-aqueous reactions were carried out in oven-dried glassware under an atmosphere of Argon. Analytical thin layer chromatography (TLC) was performed on silica gel 60, F254 plates (0.25 mm thickness) from SiliCycle. Visualization was accomplished by either irradiation under a 254 nm UV lamp or by staining with an aqueous solution of ceric ammonium molybdate (CAM). Flash chromatography was performed on silica gel 60 (230- 400 mesh). All LC-based separations involved a mobile phase of 10 mM TEAA pH 7.0 buffer (solvent A) or 0.1% formic acid aq. (solvent A) and pure acetonitrile (solvent B). HPLC separations were performed using a Varian PrepStar SD-1 solvent delivery system equipped with a Varian ProStar 335 diode array detector and a Waters Atlantis®Prep T3 column (5 µm, 19 x 150 mm), with a similarly packed guard column. LCMS separations were performed using a Waters ACQUITY UPLC system equipped with ACQUITY PDA (diode array) and FLR (fluorescence) detectors, a Waters Micromass SQD 2000 spectrometer, and a Waters ACQUITY HSS T3 column (1.8 µm, 2.1 x 100 mm). ^{1}H and ^{13}C NMR spectra were acquired on a Bruker DRX-500 spectrometer at 500 MHz and 125 MHz respectively. Chemical shifts are expressed in parts per million downfield from tetramethylsilane (TMS), using either TMS or the solvent resonance as an internal standard (TMS, ^{1}H: 0 ppm; chloroform, ^{13}C: 77.0 ppm). Data are reported as follows: chemical shift, multiplicity (s = singlet, d = doublet, t = triplet, q = quartet, m = multiplet, br = broad), coupling constant, and integration.

Chemical Synthesis

NHS Activation

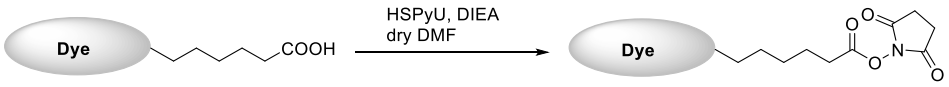

150 nmols fluorophore carboxylic acid was dissolved in 200 µL of dry DMF and then 50 µL DIEA was added to this DMF solution followed by addition of 300 nmols of dipyrrolidino(*N*-succinimidyloxy)carbenium hexafluorophosphate (HSPyU). The mixture was vortexed and then incubated in the dark at room temperature. The reaction was monitored by LCMS until completion. Once completed, the reaction solution was poured into 15 mL of ethyl acetate (EtOAc) and centrifuged. The residue was dissolved in 2 mL of 5% formic acid aq. solution and purified using a semi-preparative HPLC C18 T3 column (Waters) with a 10 mM TEAA pH 6.5 buffer mobile phase in a gradient of 10-90% acetonitrile. After evaporation of acetonitrile, the product was concentrated, buffer exchanged over a Sep-Pak C18 column and eluted with methanol and dried by rot-vap.

AC-NHS (5)

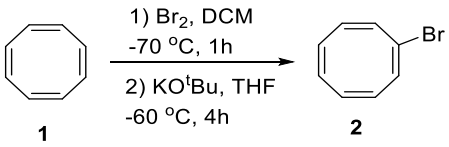

To a stirred solution of cyclooctatetraene **1** (3.0 g, 28.8 mmol) in DCM (30 ml) was slowly added a solution of Br_2 (4.6 g, 28.8 mmol) in DCM (20 mL) at -70 °C. The resulting solution was stirred at -70 °C for 1 h, at which point a solution of potassium tert-butoxide (4.5 g, 40 mmol) in THF (20 ml) was added dropwise. The reaction mixture was stirred at -60 °C for 4 h, warmed to -10 °C, and poured into ice water. Using a small amount of $MgSO_4$ to break up the emulsion, the organic layer was removed and the aqueous layer extracted with diethyl ether (3 x 20 mL). The combined extracts were dried over $MgSO_4$, filtered, and concentrated to give COT-Br **2** as a light yellow oil (5.1 g, 97%), which was used without further purification. ^{1}H NMR ($CDCl_3$): δ 6.22 (s, 1H), 5.74 – 5.98 (m, 5H), 5.62 (s, 1H); ^{13}C NMR ($CDCl_3$): δ 133.2, 133.1, 132.8, 132.4, 132.0, 130.9, 121.4.

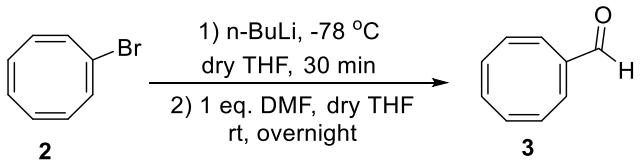

2 **3**

n-BuLi (2.5 M in hexanes) (2.2 mL, 5.46 mmol, 1.2 equiv) was added slowly at -78 °C to a solution of COT-Br **2** (1.0 g, 5.46 mmol, 1 equiv) in 20 mL THF. The resulting mixture was stirred for 30 mins at -78 °C. To this solution was added DMF (398 mg, 5.46 mmol, 1 equiv) in 2 mL dry THF. The reaction mixture was allowed to warm up to room temperature (rt) slowly and stirred overnight. The resulting solution was extracted by EtOAc and dried over Na_2SO_4. This organic solution was then filtered, and the filtrate was concentrated by evaporation under reduced pressure. The remaining crude product was purified by silica gel column using 1:5 EtOAc: Hexanes. Product aldehyde **3** (245 mg 34%) was obtained as a light-yellow oil. ^{1}H NMR ($CDCl_3$): δ 9.48 (s, 1H), 6.01-5.78 (m, 7H); ^{13}C NMR ($CDCl_3$): δ 192.6, 152.2, 144.1, 135.2, 134.7, 132.6, 131.1, 129.7, 127.4.

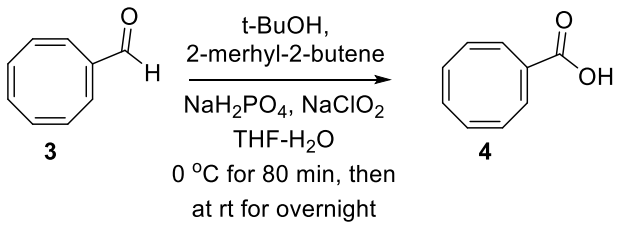

3 **4**

Aldehyde **3** (70 mg, 0.53 mmol) was dissolved in a mixture of THF (0.45mL), t-BuOH (0.45 mL), 2-methyl-2-butene (0.45 mL) and H_2O (0.15 mL). To this solution was added NaH_2PO_4 (126 mg, 1.06 mmol) at 0 °C, followed by the addition of a solution of $NaClO_2$ (78 mg, 0.689 mmol) in 0.5 mL H_2O. The reaction was stirred at 0 °C for 80 min, warmed to rt and stirred overnight. The reaction was then extracted with EtOAc, dried with Na_2SO_4 and filtered. The filtrate was concentrated under reduced pressure. The residue was purified by silica gel column using 1:3 EtOAc: Hexanes. Product acid **4** (60 mg, 76.5%) was obtained as a yellow oil. ^{1}H NMR ($CDCl_3$): δ 7.29 (s, 1H), 6.01-5.81 (m, 6H).

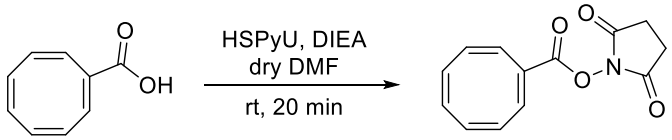

4 **5**

Acid **4** (60 mg, 0.405 mmol) was dissolved in a mixture of 2 mL dry DMF and 0.3 mL *N,N*-diisopropylethylamine (DIEA). HSPyU (333 mg, 0.81 mmol) was added to this solution. The reaction solution was stirred at rt for 20 mins. The resulting mixture was purified by silica gel column using 1:3 EtOAc: Hexanes. Product NHS ester **5** (66 mg, 66.7%) was obtained as a yellow oil. ^{1}H NMR ($CDCl_3$): δ 7.29 (s, 1H), 6.04-5.85 (m, 6H), 2.82 (s, 4H); ^{13}C NMR ($CDCl_3$): δ 169.2, 160.6, 147.6, 135.5, 135.0, 132.3, 131.5, 129.5, 129.2, 127.5, 125.6.

DAC-NHS (10)

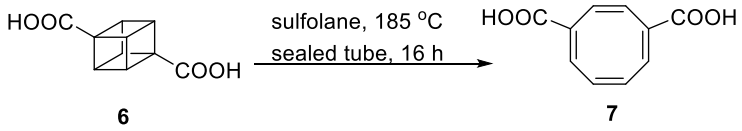

6 **7**

To a sealed tube were added 500 mg cuban-di-acid **6** and 5 mL sulfolane. This solution was heated to 185 °C for 16 h. The resulting solution was purified by using a semipreparative HPLC C18 T3 column (Waters) with a 10 mM pH 6.8 TEAA aq. mobile phase in a gradient from 10-90% acetonitrile. Pure product **7** was a brown oil (335 mg, 67%). ^{1}H NMR (MeOD-d4): δ 6.88 (s, 1H), 6.82 (s, 1H), 6.17 (s, 1H), 6.14 (s, 1H), 6.00 (s, 1H), 5.88 (d, 1H, J=8.0 Hz).

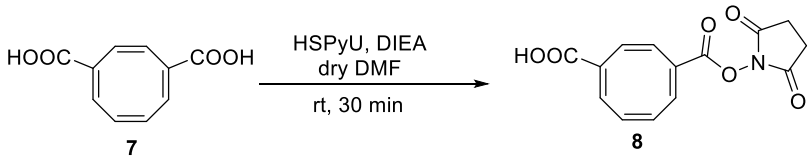

7 **8**

19 mg of COT di-acid **7** was dissolved in 1 mL dry DMF and then 50 uL of DIEA was added to this solution. While stirring, 1 eq of HSPyU (41 mg) in 1 mL dry DMF was added slowly to the di-acid solution. The resulting solution was stirred at rt for 30 min. The whole reaction was added dropwise into 0.1 mL of formic acid in 2 mL of H_2O and then was purified by using a semipreparative HPLC C18 T3 column (Waters) with a 10 mM pH 6.8 TEAA aq. mobile phase in a gradient from 10-90% acetonitrile. Pure product **8** was a brown oil (24 mg, 82%) ESI-MS: *m/z* calculated for $C_{14}H_{11}NO_6[M+H]^+$ 290.1, found 290.1.

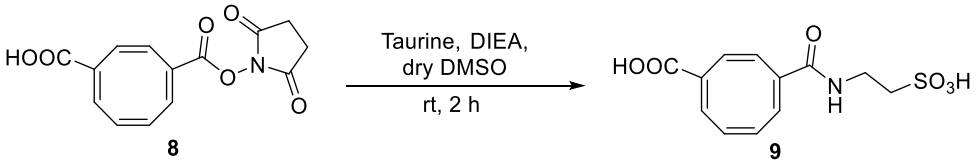

8 9

10 mg of mono ester **8** was dissolved in 2 mL of dry DMSO; 50 uL of DIEA was then added. 10 mg Taurine (2-aminoethanesulfonic acid) was added to this DMSO solution. The resulting solution was stirred at rt for 2 h and monitored by LCMS. When the reaction was complete, the DMSO solution was diluted by water and purified by using a semipreparative HPLC C18 T3 column (Waters) with a 10 mM pH 6.8 TEAA aq. mobile phase in a gradient from 10-90% acetonitrile. Pure product **9** was a brown oil (8.6 mg, 83%) ESI-MS: *m/z* calculated for $C_{12}H_{13}NO_6S$ $[M-H]^-$ 298.1, found 298.2.

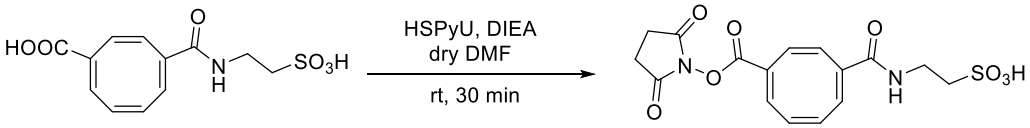

9 10

17 mg of DAC-COOH **9** was dissolved in 1 mL of dry DMF; 50 µL of DIEA was added to this solution. While stirring, 60 mg HSPyU in 1mL of dry DMF was added slowly to the di-acid solution. The resulting solution was stirred at rt for 30 min. The whole reaction was added dropwise into 0.1 mL of formic acid in 2 mL of H_2O, and then purified by using a semipreparative HPLC C18 T3 column (Waters) with a 10 mM pH 6.8 TEAA aq. mobile phase in a gradient from 10-90% acetonitrile. Pure product **10** was a brown oil (14.6mg, 65%). ESI-MS: *m/z* calculated for $C_{16}H_{16}N_2O_8S$ $[M+H]^+$ 397.1, found 397.1.

Cy3-2S-NHS (11), Cy5-2S-NHS (12) and Cy7-2S-NHS (13) (GE Healthcare Life Sciences, commercially available).

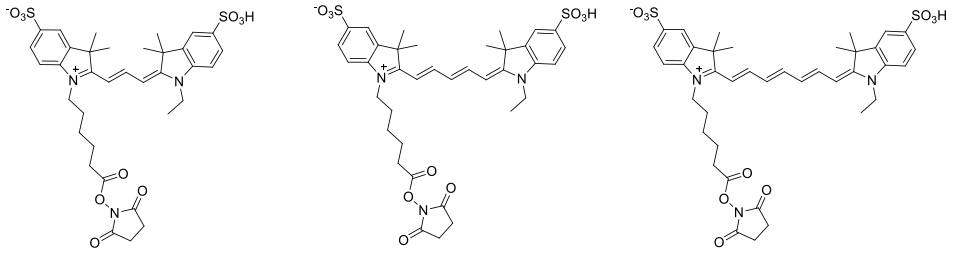

Cy3-2S-NHS 11 Cy5-2S-NHS 12 Cy7-2S-NHS 13

Cy3-2S-Me-COT (14)

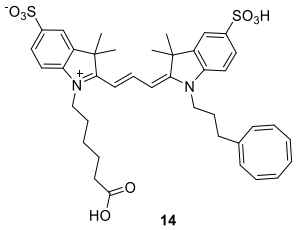

14

1-(5-carboxypentyl)-2-((E)-3-((E)-1-(3-((1Z,3Z,5Z,7Z)-cycloocta-1,3,5,7-tetraen-1-yl)propyl)-3,3-dimethyl-5-sulfoindolin-2-ylidene)prop-1-en-1-yl)-3,3-dimethyl-3H-indol-1-ium-5-sulfonate was prepared following previously published procedure (43).

Cy5-2S-Me-COT (15)

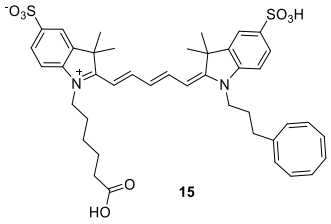

15

1-(5-carboxypentyl)-2-((1E,3E)-5-((E)-1-(3-((1Z,3Z,5Z,7Z)-cycloocta-1,3,5,7-tetraen-1-yl)propyl)-3,3-dimethyl-5-sulfoindolin-2-ylidene)penta-1,3-dien-1-yl)-3,3-dimethyl-3H-indol-1-ium-5-sulfonate was prepared following previously published procedure (43).

Cy7-2S-Me-COT (16)

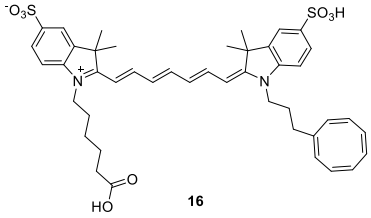

16

1-(5-carboxypentyl)-2-((1E,3E,5E)-7-((E)-1-(3-((1Z,3Z,5Z,7Z)-cycloocta-1,3,5,7-tetraen-1-yl)propyl)-3,3-dimethyl-5-sulfoindolin-2-ylidene)hepta-1,3,5-trien-1-yl)-3,3-dimethyl-3H-indol-1-ium-5-sulfonate was prepared following previously published procedure (43).

Cy3-2S-NH_2 (24)

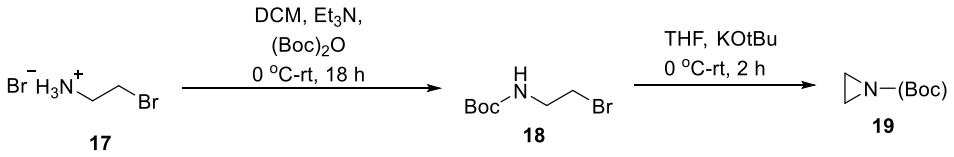

20 g of bromoamine (HBr salt) **17** was mixed with 250 mL DCM, cooled to 0 °C and then 18.8 g $(Boc)_2O$ and 17 mL of triethyl amine were added to the mixture, warmed up to rt. and stirred overnight. The reaction solution was then washed with sat. NH_4Cl aq. solution (50 mL x 4 times), then washed by brine, dried with Na_2SO_4, filtered and concentrated to yield the Boc protected product **18**. This product was carried onto the next step without further purification as a colorless oil. The Boc protected intermediate was dissolved in 150 mL of dry THF, cooled to 0 °C and then KOtBu powder (13 g) was added to this THF solution. The resulting slurry was warmed to rt. and stirred for 2 hours (h). The reaction was then quenched by 50 mL of water and extracted by Et_2O (100 mL x 3 times). Organic layers were combined, washed by water (100 mL x 8 times), washed by brine, dried over Na_2SO_4, filtered and concentrated to give the product **19** as a light-yellow oil (15.2 g, 65%). ^1H NMR ($CDCl_3$) 2.16 (s, 4H), 1.48 (s, 9H).

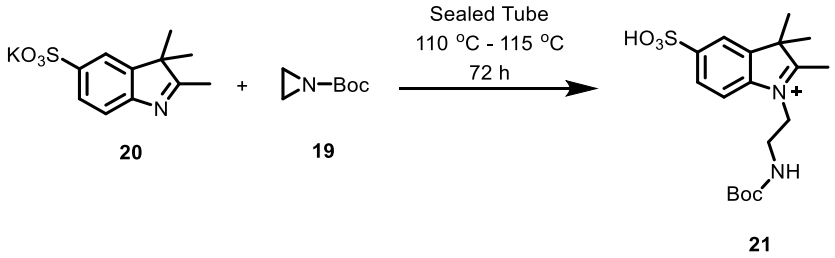

In a sealed tube were taken 1 g of indole **20** (44) and 5 g of t-butyl aziridine-1-carboxylate **19**, heated to 115 °C and stirred for 72 h. 1-2 g of fresh t-butyl aziridine-1-carboxylate was added every 24 h. The reaction tube was cooled to rt. and the slurry was then poured into 90 mL of EtOAc and centrifuged to precipitate the crude product. Pure product **21** (760 mg, 55%) was obtained by using a semipreparative HPLC C18 T3 column (Waters) with a 10 mM pH 6.8 TEAA aq. mobile phase in a gradient from 10-90% acetonitrile. ESI-MS: *m/z* calculated for $C_{18}H_{26}N_2O_5S$ $[M+H]^+$ 383.2, found 383.3.

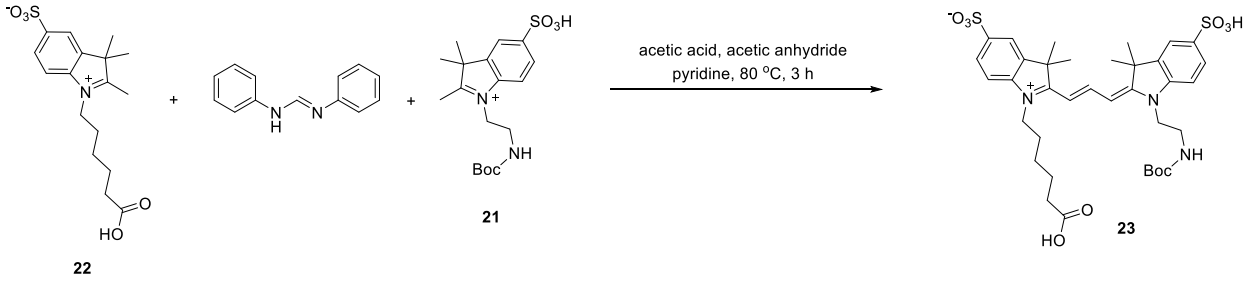

22 21 23

Indole **22** (45) (25 mg, 0.071 mmol, 1 eq.) and diphenylformimidamide (13.9 mg, 0.071 mmol, 1eq.) were dissolved in 5 mL glacial acetic acid in a 50 mL round bottom flask. 0.5 mL of acetic anhydride was added to this solution and heated to 80 °C for 2 h. After 2 hours, the reaction mixture was poured into 90 mL EtOAc to precipitate the intermediate. The intermediate was dried over vacuum, and re-dissolved in 5 mL of pyridine. Indole **21** (27.2 mg, 0.071 mmol, 1eq.) was added, followed by 0.5 mL of acetic anhydride. The final reaction solution was stirred at 80 °C for one more hour and subsequently poured into 90 mL of EtOAc to precipitate crude dye product. The precipitate was then dissolved in 10 mL of water and purified using a semipreparative HPLC C18 T3 column (Waters) with a 10 mM pH 6.8 TEAA aq. mobile phase in a gradient from 10-90% acetonitrile. After evaporation of acetonitrile, the product was concentrated and buffer exchanged over a Sep-Pak C18 column and eluted in methanol followed by evaporation in a speed vac. to give the final product **23** (9.5 mg, 17.9%) as a pinkish red solid. ESI-MS: *m/z* calculated for $C_{36}H_{47}N_3O_{10}S_2$ $[M+H]^+$ 746.3, found 746.1.

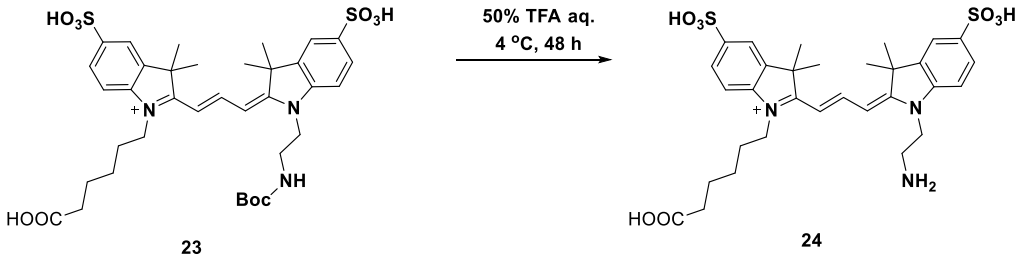

23 24

2-((E)-3-((E)-1-(2-aminoethyl)-3,3-dimethyl-5-sulfoindolin-2-ylidene)prop-1-en-1-yl)-1-(5-carboxypentyl)-3,3-dimethyl-5-sulfo-3H-indol-1-ium (24) The Boc protected Cy3 species **23** (25 mg) was dissolved 10 mL of 50% TFA aq. Solution, cooled to 4 °C and kept dark for 48 hours. The resulting dark red solution was rot-vap dried, re-dissolved in 10 mL distilled water and purified using a semipreparative HPLC C18 T3 column (Waters) with a 10 mM pH 6.8 TEAA aq. mobile phase in a gradient from 10-90% acetonitrile. After evaporation of acetonitrile, the product was concentrated and buffer exchanged over a Sep-Pak C18 column and eluted in methanol followed

by evaporation in a speed vac. to give the final product **24** (18.8 mg, 87%) as a pinkish red solid. ESI-MS: *m/z* calculated for $C_{31}H_{39}N_3O_8S_2$ $[M+H]^+$ 646.2, found 646.3.

Cy5-2S-NH$_2$ (25)

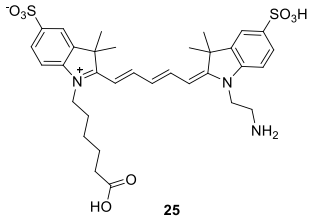

25

2-((1E,3E)-5-((E)-1-(2-aminoethyl)-3,3-dimethyl-5-sulfoindolin-2-ylidene)penta-1,3-dien-1-yl)-1-(5-carboxypentyl)-3,3-dimethyl-3H-indol-1-ium-5-sulfonate (25) was prepared following previous published procedures (41).

Cy7-2S-NH$_2$ (27)

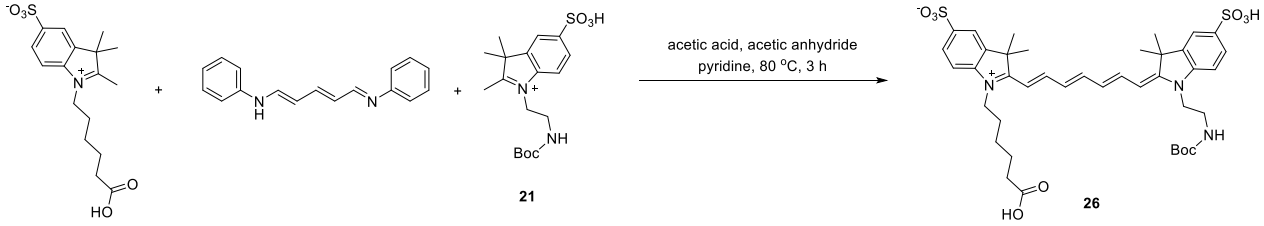

Indole **22** (25 mg, 0.071 mmol, 1 eq.) and glutaconaldehydedianil hydrochloride (20 mg, 0.71 mmol, 1eq.) were dissolved in 5 mL glacial acetic acid in a 50 mL round bottom flask. 0.5 mL acetic anhydride was added to this solution and then heated to 80 ^oC for 2 h. After 2 hours, the reaction mixture was poured into 90 mL EtOAc to precipitate the intermediate. The intermediate was dried over vacuum, and re-dissolved in 5 mL of pyridine. indole **21** (27.2 mg, 0.071 mmol, 1eq.) was added, followed by 0.5 mL of acetic anhydride. The final reaction solution was stirred at 80 ^oC for one more hour before pouring into 90 mL of EtOAc to precipitate crude dye product. The precipitate was then dissolved in 10 mL of water purified using a semipreparative HPLC C18 T3 column (Waters) with a 10 mM pH 6.8 TEAA aq. mobile phase in a gradient from 10-90% acetonitrile. After evaporation of acetonitrile, the product was concentrated and buffer exchanged over a Sep-Pak C18 column and eluted in methanol followed by evaporation in a speed vac. to give the final product **26** (11.3 mg, 20%) as a teal colored solid. ESI-MS: *m/z* calculated for $C_{40}H_{51}N_3O_{10}S_2$ $[M+H]^+$ 798.3, found 798.4.

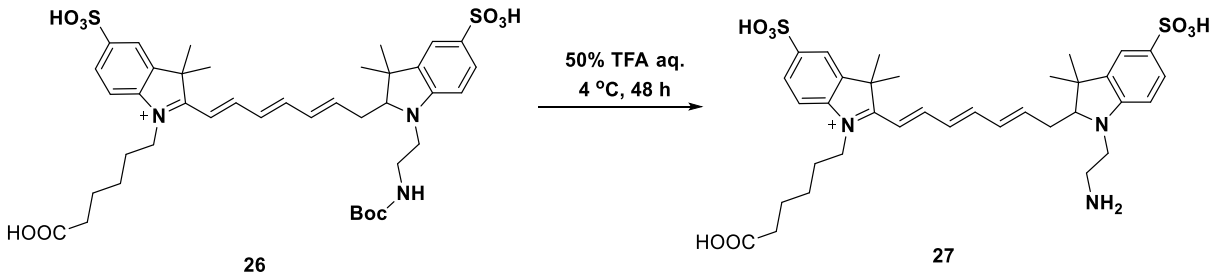

2-((1E,3E,5E)-7-(1-(2-aminoethyl)-3,3-dimethyl-5-sulfoindolin-2-yl)hepta-1,3,5-trien-1-yl)-1-(5-carboxypentyl)-3,3-dimethyl-5-sulfo-3H-indol-1-ium (27). The Boc protected Cy7 species **26** (25 mg) was dissolved in 10 mL of 50% TFA aq. Solution, cooled to 4 °C and kept dark for 48 hours. The resulting dark red solution was rot-vap dried, re-dissolved in 10 mL distilled water and purified using a semipreparative HPLC C18 T3 column (Waters) with a 10 mM pH 6.8 TEAA aq. mobile phase in a gradient from 10-90% acetonitrile. After evaporation of acetonitrile, the product was concentrated and buffer exchanged over a Sep-Pak C18 column and eluted in methanol followed by evaporation in a speed vac. to give the final product **27** (21.8 mg, 85%) as a teal solid. ESI-MS: *m/z* calculated for $C_{35}H_{45}N_3O_8S_2$ $[M+H]^+$ 700.3, found 700.5.

Cy3-4S-Me-COT (31)

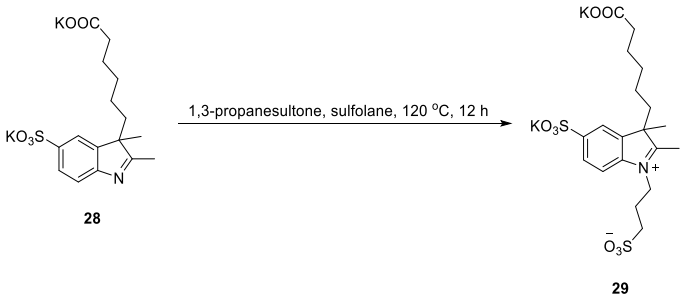

In a sealed tube were taken 50 mg of compound **28** (46) and 1mL of sulfolane followed by addition of 100 mg of 1,3-propanesultone. The reaction was heated to 120 °C for 12 h, then poured into 40 mL EtOAc to precipitate crude product. The product **29** was carried onto the next step without further purification. ESI-MS *m/z* calculated for $C_{19}H_{25}K_2NO_8S_2$ $[M - 2K + H]^-$: 460.1, found: 460.3.

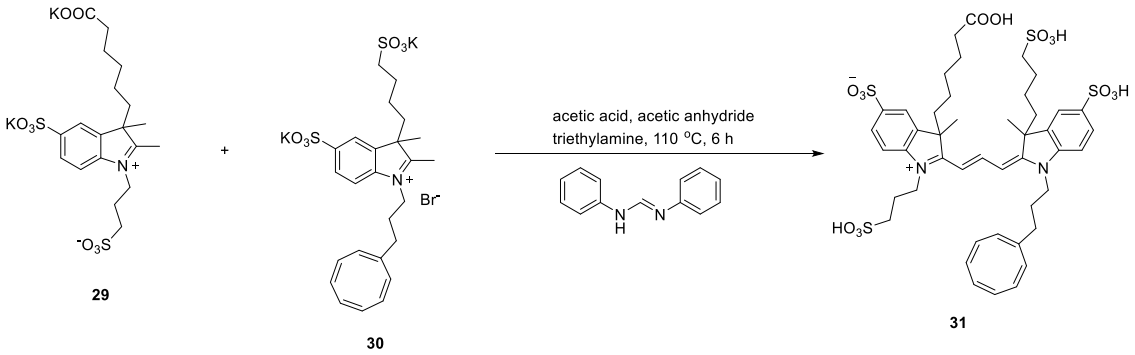

3-(5-carboxypentyl)-2-((1E,3E)-5-((E)-1-(3-((1Z,3Z,5Z,7Z)-cycloocta-1,3,5,7-tetraen-1-yl)propyl)-3-methyl-5-sulfo-3-(4-sulfobutyl)indolin-2-ylidene)penta-1,3-dien-1-yl)-3-methyl-1-(3-sulfopropyl)-3H-indol-1-ium-5-sulfonate (31). Indole **29** (54 mg. 0.1 mmol, 1eq.) was dissolved in 2 mL acetic acid and then diphenylformimidamide (19 mg, 0.1 mmol, 1 eq.) and 0.4 mL acetic anhydride were added. The reaction mixture was heated to 110 °C for 3 h and poured into 40 mL EtOAc. The precipitate was then dried, mixed with compound **30** (43) (66 mg), and then 2 mL acetic acid was added, followed by 0.3 mL of trimethylamine. The purple solution was heated to 80 °C for another 3 h as the color of the solution turned from purple to dark red. The resulting solution was poured into 40 mL of EtOAc and the residue was purified by reversed phase C18 column using 10mM TEAA pH7.0 aq. – acetonitrile as solvent. Pure compound **31** (24.4 mg) was obtained as a red-colored solid at 25% yield. ESI-MS *m/z* calculated for $C_{45}H_{56}N_2O_{14}S_4$ $[M-2H]^{2-}/2$: 487.2, found: 487.1.

Cy5-4S-Me-COT (32)

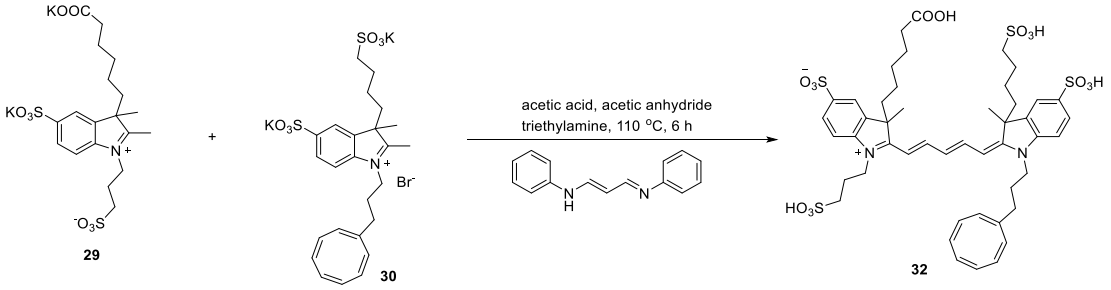

3-(5-carboxypentyl)-2-((1E,3E)-5-((E)-1-(3-((1Z,3Z,5Z,7Z)-cycloocta-1,3,5,7-tetraen-1-yl)propyl)-3-methyl-5-sulfo-3-(4-sulfobutyl)indolin-2-ylidene)penta-1,3-dien-1-yl)-3-methyl-1-(3-sulfopropyl)-3H-indol-1-ium-5-sulfonate (32). Indole **29** (54 mg, 0.1 mmol, 1eq.) was dissolved in 2 mL acetic acid and then malonaldehyde dianilide hydrochloride (26 mg, 0.1 mmol, 1 eq.) and 0.4 mL acetic anhydride were added. The reaction mixture was heated to 110 °C for 3

h and poured into 40 mL EtOAc. The precipitate was then dried, mixed with compound **30** (66 mg) and then 2 mL acetic acid was added, followed by 0.3 mL of trimethylamine. The purple solution was heated up 80 ^{o}C for another 3 h, during the heating, the color of the solution turned from purple to dark blue. The resulting solution was poured into 40 mL of EtOAc, the residue was purified by reversed phase C18 column using 10 mM TEAA pH7.0 aq. – acetonitrile as solvent. Pure compound **32** (27mg) was obtained as a blue-colored solid and the yield was 27%. ESI-MS *m/z* calculated for $C_{47}H_{58}N_2O_{14}S_4$ $[M-2H]^{2-}/2$: 500.2, found: 500.2.

Cy7-4S-Me-COT (33)

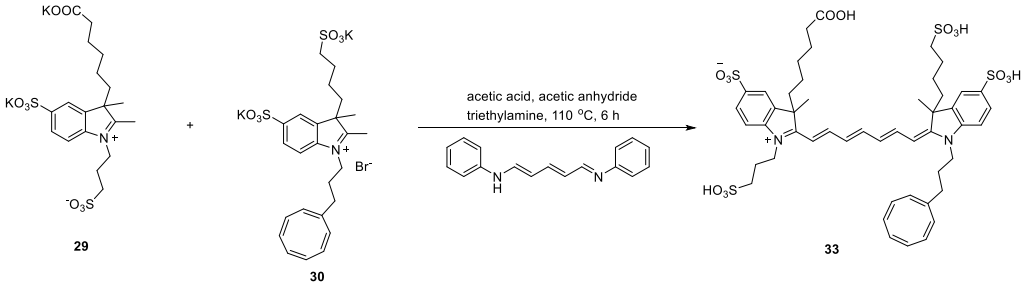

3-(5-carboxypentyl)-2-((1E,3E,5E)-7-((E)-1-(3-((1Z,3Z,5Z,7Z)-cycloocta-1,3,5,7-tetraen-1-yl)propyl)-3-methyl-5-sulfo-3-(4-sulfobutyl)indolin-2-ylidene)hepta-1,3,5-trien-1-yl)-3-methyl-1-(3-sulfopropyl)-3H-indol-1-ium-5-sulfonate (33). Indole **29** (54 mg, 0.1 mmol, 1eq.) was dissolved in 2 mL acetic acid, glutaconaldehdedianil hydrochloride (28 mg, 0.1 mmol, 1 eq.) and 0.4 mL acetic anhydride were added. The reaction mixture was heated to 110 ^{o}C for 3 h and poured into 40 mL of EtOAc. The precipitate was then dried, mixed with compound **30** (66 mg), and then 2 mL acetic acid was added, followed by 0.3 mL of trimethylamine. The purple solution was heated to 80 ^{o}C for another 3 h with the color of the solution turning from purple to green. The resulting solution was poured into 40 mL of EtOAc and the residue was purified by reversed phase C18 column using 10mM TEAA pH7.0 aq. – acetonitrile as solvent. Pure compound **33** (33 mg) was obtained as a teal-colored solid, at 33% yield. ESI-MS *m/z* calculated for $C_{49}H_{60}N_2O_{14}S_4$ $[M-2H]^{2-}/2$: 513.2, found: 513.1.

Cy3-4S-NH$_2$ (38)

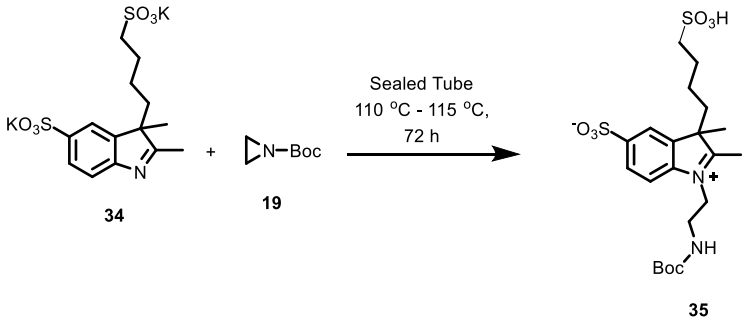

In a sealed tube were taken 1 g of indole **34** (47) and 5 g of t-butyl aziridine-1-carboxylate **19**, heated to 115 °C and stirred for 72 h with 1-2 g of fresh t-butyl aziridine-1-carboxylate was added every 24 h. The reaction tube was cooled to rt., poured into 90 mL of EtOAc and centrifuged to precipitate the crude product. Pure product **35** (483 mg, 45%) was obtained by using a semipreparative HPLC C18 T3 column (Waters) with a 10 mM pH 6.8 TEAA aq. mobile phase in a gradient from 10-90% acetonitrile. ESI-MS: *m/z* calculated for $C_{21}H_{32}N_2O_8S_2$ $[M-H]^-$ 503.6, found 503.5.

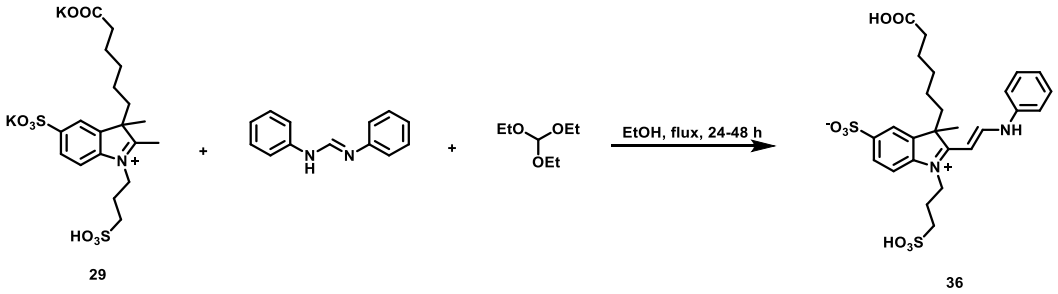

Indole **29** (53 mg, 0.1 mmol, 1 eq.) was taken in 35 mL of EtOH, *N,N'*-diphenylformamidine (20 mg, 0.1 mmol, 1eq.) and 2 mL of triethyl orthoformate were added to this solution. The reaction mixture was heated to 85 °C and refluxed for 24-48 h while monitoring by LCMS until the conversion was complete. The dark brown solution was then poured into 90 mL of EtOAc and centrifuged to precipitate the crude product. The crude product was then dissolved in 20 mL of 1:1 H_2O and acetonitrile, sonicated for 10 mins, and filtered. The pure product **36** (42 mg, 75%) was obtained by using a semipreparative HPLC C18 T3 column (Waters) with a 10 mM pH 6.8 TEAA aq. mobile phase in a gradient from 10-90% acetonitrile. ESI-MS: *m/z* calculated for $C_{26}H_{32}N_2O_8S_2$ $[M-H]^-$ 563.2, found 563.1.

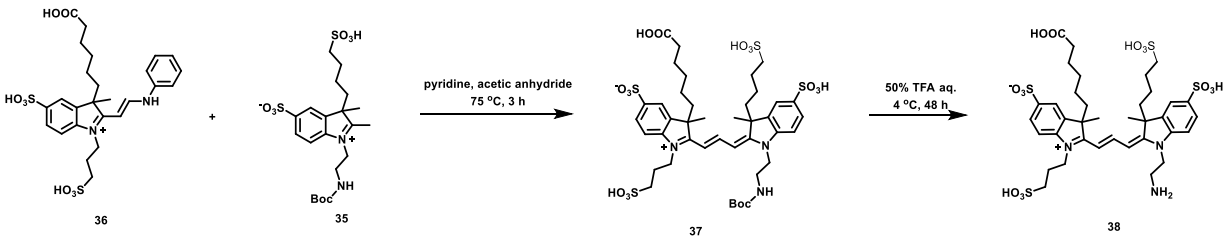

2-((E)-3-((E)-1-(2-aminoethyl)-3-methyl-5-sulfo-3-(4-sulfobutyl)indolin-2-ylidene)prop-1-en-1-yl)-3-(5-carboxypentyl)-3-methyl-1-(3-sulfopropyl)-3H-indol-1-ium-5-sulfonate (38). Intermediate **36** (28 mg, 0.05 mmol, 1eq.) and Boc protected indole species **35** (25 mg, 0.05 mmol, 1eq.) were dissolved in 10 mL of pyridine, and then to this dark brown solution was added 1.5 mL of acetic anhydride. The reaction was then heated to 85 °C for 3 h and monitored by LCMS. When the reaction was complete, the solution turned to very intense pinkish color. The crude reaction solution was then poured into 90 mL of EtOAc and centrifuged to precipitate the crude dye product. The pink-red solid was then dissolved in water, transferred to an rbf and rot-vap dried. The resulting red solid **37** was again dissolved in 15 mL of 50% TFA aq. Solution and kept in the dark at 4 °C for 48 h to fully hydrolyze all the protecting groups. The reaction solution was then rot-vaped to remove TFA and water. The resulting red solid was re-dissolved in 10 mL of H_2O, purified by using a semipreparative HPLC C18 T3 column (Waters) with a 10 mM pH 6.8 TEAA aq. mobile phase in a gradient from 10-90% acetonitrile. Product **38** (7.8 mg, 18%) was a red solid. ESI-MS: *m/z* calculated for $C_{36}H_{49}N_3O_{14}S_4$ $[M-H]^-$ 874.2, found 874.5.

Cy5-4S-NH$_2$ (41)

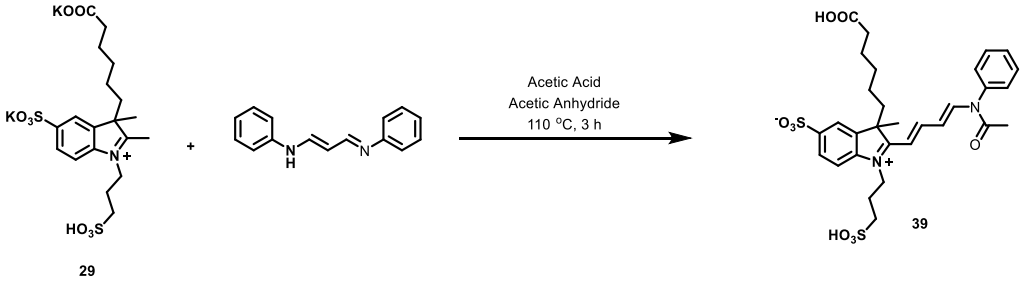

Indole species **29** (54 mg, 0.1 mmol, 1 eq.) was taken in 15 mL of acetic acid and 2 mL of acetic anhydride, 30 mg of glutaconaldehdedianil hydrochloride was added to this solution. The reaction solution was then heated to 110 °C for 3 h and monitored by LCMS every hour. The dark brown solution was then poured into 90 mL of EtOAc and centrifuged to precipitate the crude product.

The crude product was then dissolved in 20 mL of 1:1 H_2O and acetonitrile, sonicated for 10 mins, and filtered. The pure product **39** (48 mg, 76%) was obtained by using a semipreparative HPLC C18 T3 column (Waters) with a 10 mM pH 6.8 TEAA aq. mobile phase in a gradient from 10-90% acetonitrile. ESI-MS: *m/z* calculated for $C_{30}H_{36}N_2O_9S_2$ $[M-H]^-$ 631.2, found 631.2.

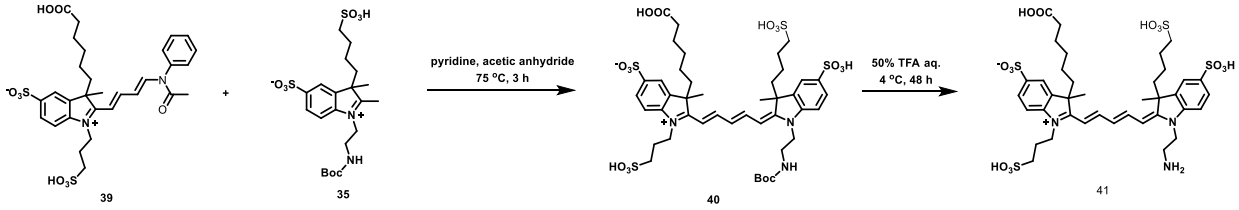

2-((1E,3E)-5-((E)-1-(2-aminoethyl)-3-methyl-5-sulfo-3-(4-sulfobutyl)indolin-2-ylidene)penta-1,3-dien-1-yl)-3-(5-carboxypentyl)-3-methyl-1-(3-sulfopropyl)-3H-indol-1-ium-5-sulfonate (41). Intermediate **39** (32 mg, 0.05 mmol, 1eq.) and Boc protected indole species **35** (25 mg, 0.05 mmol, 1eq.) were dissolved in 10 mL of pyridine, and then to this dark brown solution 1.5 mL of acetic anhydride was added, heated to 85 °C for 3 h, and monitored by LCMS. When the reaction was complete, the solution turned to very intense blue color. The crude reaction solution was then poured into 90 mL of EtOAc and centrifuged to precipitate the crude dye product. The blue solid was then dissolved in water, transferred to an rbf and rot-vap dried. The resulting blue solid **40** was again dissolved in 15 mL of 50% TFA aq. Solution and kept in the dark at 4 °C for 48 h to fully hydrolyze all the protecting groups. The reaction solution was then rot-vaped to remove TFA and water. The resulting blue solid was re-dissolved in 10 mL of H_2O and purified using a semipreparative HPLC C18 T3 column (Waters) with a 10 mM pH 6.8 TEAA aq. mobile phase in a gradient from 10-90% acetonitrile. Product **41** (11.7 mg, 26%) was a blue solid. ESI-MS: *m/z* calculated for $C_{38}H_{51}N_3O_{14}S_4$ $[M-H]^-$ 900.2, found 900.1.

Cy7-4S-NH_2 (44)

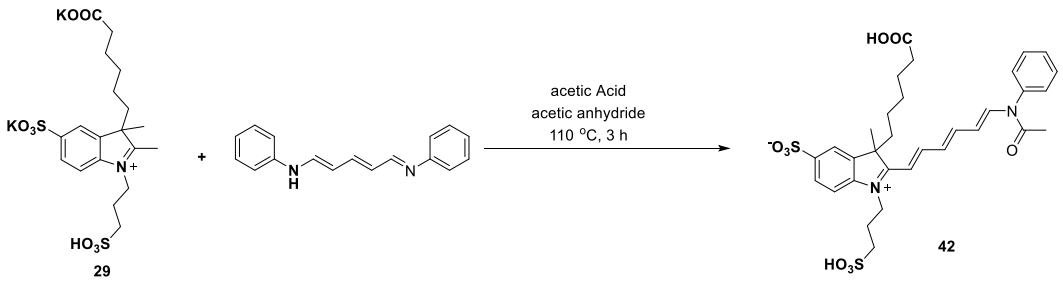

Indole species **29** (54 mg, 0.1 mmol, 1eq.) was taken in 15 mL of acetic acid and 2 mL of acetic anhydride. (28 mg, 0.1 mmol, 1eq.) of malonaldehyde dianilide hydrochloride was added to this

solution and heated to 110 °C for 3 h, monitored by LCMS every hour. The dark brown solution was then poured into 90 mL of EtOAc and centrifuged to precipitate the crude product. The crude product was then dissolved in 20 mL of 1:1 H_2O and acetonitrile, sonicated for 10 mins and filtered. The pure product **42** (45 mg, 68%) was obtained using a semipreparative HPLC C18 T3 column (Waters) with a 10 mM pH 6.8 TEAA aq. mobile phase in a gradient from 10-90% acetonitrile. ESI-MS: *m/z* calculated for $C_{32}H_{38}N_2O_9S_2$ $[M-H]^-$ 657.2, found 657.0.

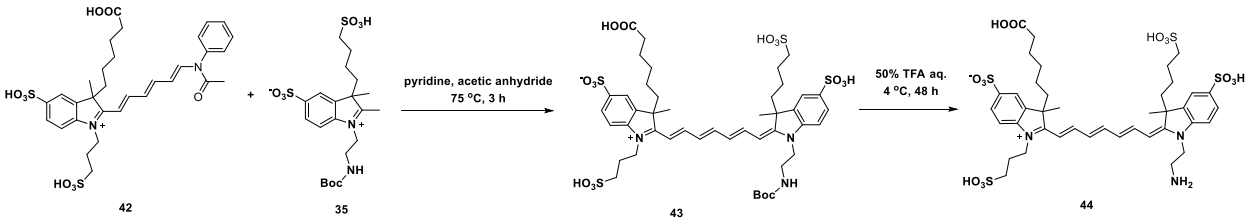

2-((1E,3E,5E)-7-((E)-1-(2-aminoethyl)-3-methyl-5-sulfo-3-(4-sulfobutyl)indolin-2-ylidene)hepta-1,3,5-trien-1-yl)-3-(5-carboxypentyl)-3-methyl-1-(3-sulfopropyl)-3H-indol-1-ium-5-sulfonate (44). Intermediate **42** (33 mg, 0.05 mmol, 1eq.) and Boc protected indole species **35** (25 mg, 0.05 mmol, 1 eq.) were dissolved in 10 mL of pyridine, and then to this dark brown solution was added 1.5 mL of acetic anhydride. The reaction was then heated to 85 °C for 3 h and monitored by LCMS. When the reaction was complete, the solution turned to very intense teal color. The crude reaction solution was then poured into 90 mL of EtOAc and centrifuged to precipitate the crude dye product. The teal solid was then dissolved in water, transferred to a rbf and rot-vap dried. The resulting blue solid **43** was again dissolved in 15 mL of 50% TFA aq. Solution and kept in the dark at 4 °C for 48 h to fully hydrolyze all the protecting groups. The reaction solution was then rot-vaped to remove TFA and water. The resulting red solid was re-dissolved in 10 mL of H_2O and purified using a semipreparative HPLC C18 T3 column (Waters) with a 10 mM pH 6.8 TEAA aq. mobile phase in a gradient from 10-90% acetonitrile. Product **44** (16.2 mg, 35%) was a teal colored solid. ESI-MS: *m/z* calculated for $C_{40}H_{53}N_3O_{14}S_4$ $[M-H]^-$ 926.2, found 926.3.

Dye-NH_2 Coupled with AC-NHS or DAC-NHS General Procedure

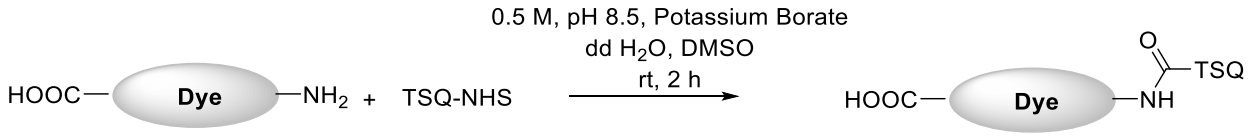

1 mmol of amino dye was dissolved in 2 mL of ddH_2O. To this solution was added 1 mL DMSO and 320 µL of 0.5M pH 8.1 potassium borate buffer solution. TSQ-NHS (4 mmol, 4 eq.) was dissolved in 1 mL of dry DMSO and added to the dye-NH_2 solution slowing while stirring. The resulting reaction solution was stirred at rt for 20 – 40 mins and monitored by LCMS. The crude product was purified using a semipreparative HPLC C18 T3 column (Waters) with a 10 mM pH 6.8 TEAA aq. mobile phase in a gradient from 10-90% acetonitrile.

Cy3-4S-AC (45)

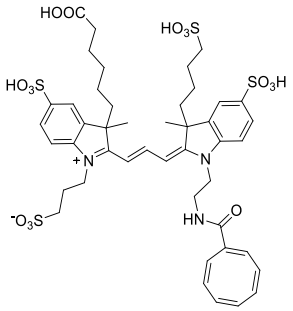

45

3-(3-(5-carboxypentyl)-2-((E)-3-((E)-1-(2-((1E,3Z,5Z,7Z)-cycloocta-1,3,5,7-tetraene-1-carboxamido)ethyl)-3-methyl-5-sulfo-3-(4-sulfobutyl)indolin-2-ylidene)prop-1-en-1-yl)-3-methyl-5-sulfo-3H-indol-1-ium-1-yl)propane-1-sulfonate

ESI-MS: *m/z* calculated for $C_{45}H_{55}N_3O_{15}S_4$ $[M-2H]^{2-}/2$ 501.7, found 501.6.

Cy5-4S-AC (46)

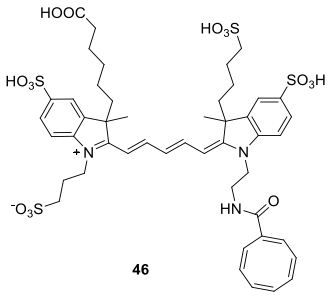

46

3-(3-(5-carboxypentyl)-2-((1E,3E)-5-((E)-1-(2-((1E,3Z,5Z,7Z)-cycloocta-1,3,5,7-tetraene-1-carboxamido)ethyl)-3-methyl-5-sulfo-3-(3-sulfopropyl)indolin-2-ylidene)penta-1,3-dien-1-yl)-3-methyl-5-sulfo-3H-indol-1-ium-1-yl)propane-1-sulfonate

ESI-MS: *m/z* calculated for $C_{47}H_{57}N_3O_{15}S_4$ $[M-2H]^{2-}/2$ 514.6, found 514.8.

Cy7-4S-AC (47)

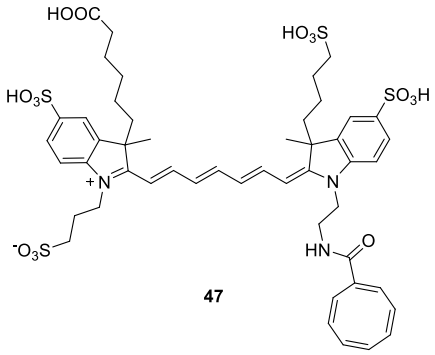

3-(3-(5-carboxypentyl)-2-((1E,3E,5E)-7-((E)-1-(2-((1E,3Z,5Z,7Z)-cycloocta-1,3,5,7-tetraene-1-carboxamido)ethyl)-3-methyl-5-sulfo-3-(4-sulfobutyl)indolin-2-ylidene)hepta-1,3,5-trien-1-yl)-3-methyl-5-sulfo-3H-indol-1-ium-1-yl)propane-1-sulfonate

ESI-MS: *m/z* calculated for $C_{49}H_{59}N_3O_{15}S_4$ $[M-2H]^{2-}/2$ 527.7, found 527.8.

Cy3-4S-DAC (48)

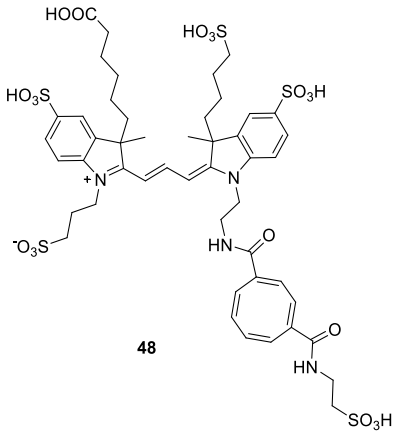

3-(3-(5-carboxypentyl)-3-methyl-2-((E)-3-((E)-3-methyl-5-sulfo-3-(4-sulfobutyl)-1-(2-((1E,3E,5Z,7Z)-4-((2-sulfoethyl)carbamoyl)cycloocta-1,3,5,7-tetraene-1-carboxamido)ethyl)indolin-2-ylidene)prop-1-en-1-yl)-5-sulfo-3H-indol-1-ium-1-yl)propane-1-sulfonate

ESI-MS: *m/z* calculated for $C_{48}H_{60}N_4O_{19}S_5$ $[M-2H]^{2-}/2$ 577.2, found 577.3.

Cy5-4S-DAC (49)

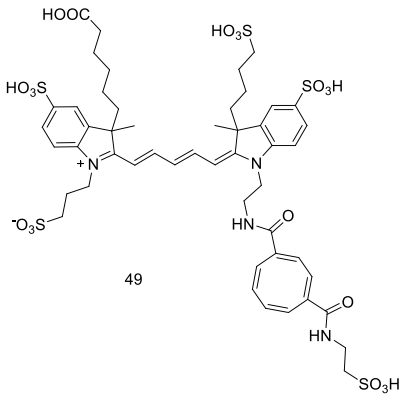

3-(3-(5-carboxypentyl)-3-methyl-2-((1E,3E)-5-((E)-3-methyl-5-sulfo-3-(4-sulfobutyl)-1-(2-((1E,3E,5Z,7Z)-4-((2-sulfoethyl)carbamoyl)cycloocta-1,3,5,7-tetraene-1-carboxamido)ethyl)indolin-2-ylidene)penta-1,3-dien-1-yl)-5-sulfo-3H-indol-1-ium-1-yl)propane-1-sulfonate

ESI-MS: *m/z* calculated for $C_{50}H_{62}N_4O_{19}S_5$ $[M-2H]^{2-}/2$ 590.2, found 590.1.

Cy7-4S-DAC (50)

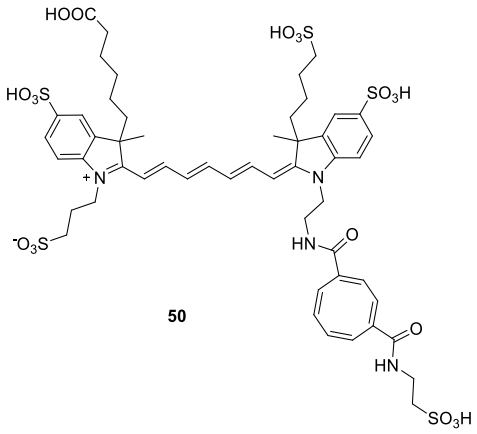

3-(3-(5-carboxypentyl)-3-methyl-2-((1E,3E,5E)-7-((E)-3-methyl-5-sulfo-3-(4-sulfobutyl)-1-(2-((1E,3E,5Z,7Z)-4-((2-sulfoethyl)carbamoyl)cycloocta-1,3,5,7-tetraene-1-carboxamido)ethyl)indolin-2-ylidene)hepta-1,3,5-trien-1-yl)-5-sulfo-3H-indol-1-ium-1-yl)propane-1-sulfonate

ESI-MS: *m/z* calculated for $C_{52}H_{64}N_4O_{19}S_5$ $[M-2H]^{2-}/2$ 603.2, found 603.5.

References

1. Frisch MJ, Trucks GW, Schlegel HB, Scuseria GE, Wallingford Gaussian 16, revision A. 03.

2. Zhao Y, Truhlar DG (2008) The M06 suite of density functionals for main group thermochemistry, thermochemical kinetics, noncovalent interactions, excited states, and transition elements: two new functionals and systematic testing of four M06-class functionals and 12 other functionals. *Theor Chem Acc* 120(1-3):215–241.

3. Tomasi J, Mennucci B, Cammi R (2005) Quantum mechanical continuum solvation models. *Chem Rev* 105(8):2999–3093.

4. Handy NC, Cohen AJ (2001) Left-right correlation energy. *Mol Phys* 99(5):403–412.

5. Hoe W-M, Cohen AJ, Handy NC (2001) Assessment of a new local exchange functional OPTX. *Chem Phys Lett* 341(3-4):319–328.

6. Lee C, Yang W, Parr RG (1988) Development of the Colle-Salvetti correlation-energy formula into a functional of the electron density. *Phys Rev B, Condens Matter* 37(2):785–789.

7. Grimme S, Antony J, Ehrlich S, Krieg H (2010) A consistent and accurate ab initio parametrization of density functional dispersion correction (DFT-D) for the 94 elements H-Pu. *J Chem Phys* 132(15):154104.

8. El Seoud OA, Baader WJ, Bastos EL (2016) in *Encyclopedia of physical organic chemistry, 5 volume set*, ed Wang Z (John Wiley & Sons, Inc., Hoboken, NJ, USA), pp 1–68.

9. Krygowski TM (1993) Crystallographic studies of inter- and intramolecular interactions reflected in aromatic character of .pi.-electron systems. *J Chem Inf Model* 33(1):70–78.

10. Krygowski TM, Cyrański M (1996) Separation of the energetic and geometric contributions to the aromaticity of π-electron carbocyclics. *Tetrahedron* 52(5):1713–1722.

11. Krygowski TM, Cyrański MK (2001) Structural aspects of aromaticity. *Chem Rev* 101(5):1385–1420.

12. Bultinck P, et al. (2006) Electron delocalization and aromaticity in linear polyacenes: atoms in molecules multicenter delocalization index. *J Phys Chem A* 110(24):7642–7648.

13. Matito E, Duran M, Solà M (2005) The aromatic fluctuation index (FLU): a new aromaticity index based on electron delocalization. *J Chem Phys* 122(1):14109.

14. Schleyer P von R, Maerker C, Dransfeld A, Jiao H, van Eikema Hommes NJR (1996) Nucleus-Independent Chemical Shifts: A Simple and Efficient Aromaticity Probe. *J Am Chem Soc* 118(26):6317–6318.

15. Wolinski K, Hinton JF, Pulay P (1990) Efficient implementation of the gauge-independent atomic orbital method for NMR chemical shift calculations. *J Am Chem Soc* 112(23):8251–8260.

16. Gershoni-Poranne R, Stanger A (2014) The NICS-XY-scan: identification of local and global ring currents in multi-ring systems. *Chem Eur J* 20(19):5673–5688.

17. Rahalkar A, Stanger A Aroma. Available at: http://schulich.technion.ac.il/Amnon_Stanger.htm [Accessed July 1, 2018].

18. Herges R, Geuenich D (2001) Delocalization of electrons in molecules†. *J Phys Chem A* 105(13):3214–3220.

19. Geuenich D, Hess K, Köhler F, Herges R (2005) Anisotropy of the induced current density (ACID), a general method to quantify and visualize electronic delocalization. *Chem Rev* 105(10):3758–3772.

20. Matito E (2006) *ESI-3D: Electron sharing indexes program for 3D molecular space partitioning* (Institute of Computational Chemistry and Catalysis, Girona, Catalonia, Spain. http://iqc.udg.es/~eduard/ESI).

21. Keith TA (2018) *AIMAll (Version 17.11.14.B)* (TK Gristmill Software, Overland Park, KS, US. http://aim.tkgristmill.com).

22. Becke AD (1993) Density-functional thermochemistry. III. The role of exact exchange. *J Chem Phys* 98(7):5648.

23. Baboul AG, Curtiss LA, Redfern PC, Raghavachari K (1999) Gaussian-3 theory using density functional geometries and zero-point energies. *J Chem Phys* 110(16):7650–7657.

24. Curtiss LA, Redfern PC, Raghavachari K (2007) Gaussian-4 theory using reduced order perturbation theory. *J Chem Phys* 127(12):124105.

25. Zheng Q, et al. (2016) Intra-molecular triplet energy transfer is a general approach to improve organic fluorophore photostability. *Photochem Photobiol Sci* 15(2):196–203.

26. Yagci Y, Jockusch S, Turro NJ (2007) Mechanism of Photoinduced Step Polymerization of Thiophene by Onium Salts: Reactions of Phenyliodinium and Diphenylsulfinium Radical Cations with Thiophene. *Macromolecules* 40(13):4481–4485.

27. Juette MF, et al. (2016) Single-molecule imaging of non-equilibrium molecular ensembles on the millisecond timescale. *Nat Methods* 13(4):341–344.

28. Qin F (2004) Restoration of single-channel currents using the segmental k-means method based on hidden Markov modeling. *Biophys J* 86(3):1488–1501.

29. Deerinck TJ, et al. (1994) Fluorescence photooxidation with eosin: a method for high resolution immunolocalization and in situ hybridization detection for light and electron microscopy. *J Cell Biol* 126(4):901–910.

30. Lakowicz JR ed. (2006) in *Principles of fluorescence spectroscopy* (Springer US, Boston, MA), pp 797–840.

31. Prakash V, et al. (2019) Ribosome biogenesis during cell cycle arrest fuels EMT in development and disease. *Nat Commun* 10(1):2110.

32. Chino S, Sakaguchi A, Yamoto R, Ferri S, Sode K (2007) Branched-chain Amino Acid Biosensing Using Fluorescent Modified Engineered Leucine/Isoleucine/Valine Binding Protein. *ijms* 8(6):513–525.

33. Fitzgerald GA, et al. (2019) Quantifying secondary transport at single-molecule resolution. *Nature* 575(7783):528–534.

34. Roy R, Hohng S, Ha T (2008) A practical guide to single-molecule FRET. *Nat Methods* 5(6):507–516.

35. Reichel A, et al. (2007) Noncovalent, site-specific biotinylation of histidine-tagged proteins. *Anal Chem* 79(22):8590–8600.

36. Müller BK, Zaychikov E, Bräuchle C, Lamb DC (2005) Pulsed interleaved excitation. *Biophys J* 89(5):3508–3522.

37. Schuler B (2007) Application of single molecule Förster resonance energy transfer to protein folding. *Methods Mol Biol* 350:115–138.

38. Eggeling C, et al. (2001) Data registration and selective single-molecule analysis using multi-parameter fluorescence detection. *J Biotechnol* 86(3):163–180.

39. Hoffmann A, et al. (2011) Quantifying heterogeneity and conformational dynamics from single molecule FRET of diffusing molecules: recurrence analysis of single particles (RASP). *Phys Chem Chem Phys* 13(5):1857–1871.

40. Altman RB, et al. (2011) Cyanine fluorophore derivatives with enhanced photostability. *Nat Methods* 9(1):68–71.

41. Zheng Q, et al. (2017) Electronic tuning of self-healing fluorophores for live-cell and single-molecule imaging. *Chem Sci* 8(1):755–762.

42. Turro NJ, Ramamurthy V, Scaiano JC (2010) *Modern Molecular Photochemistry of Organic Molecules* (University Science Books).

43. WO2013109859A1 - Dye compositions, methods of preparation, conjugates thereof, and methods of use - Google Patents Available at: https://patents.google.com/patent/WO2013109859A1/en?oq=Blanchard%2c+S.+C.%2c+Altman%2c+R.%2c+Warren%2c+J.+D.+%26+Zhou%2c+Z.+PCT+Int.+Appl.%2c+20131098 59%2c+25+Jul+2013 [Accessed July 13, 2020].

44. Sugahara A, Tanaka N, Okazawa A, Matsushita N, Kojima N (2014) Photochromic Property of Anionic Spiropyran with Sulfonate-substituted Indoline Moiety. *Chem Lett* 43(3):281–283.

45. WO2009014513A1 - Novel dyes for the detection or quantification of desirable target molecules - Google Patents Available at: https://patents.google.com/patent/WO2009014513A1/en?oq=Pande%2c+P.%2c+Szczepanik%2c+M.+%26+Xiang%2c+Y-J.+PCT+Int.+Appl.%2c+2009014513%2c+29+Jan+2009 [Accessed July 13, 2020].

46. WO2004039894A3 - Chiral indole intermediates and their fluorescent cyanine dyes containing functional groups - Google Patents Available at: https://patents.google.com/patent/WO2004039894A3/en?oq=Mujumdar%2c+R.+B.+%26+West%2c+R.+M.+PCT+Int.+Appl.%2c+2004039894%2c+13+May+2004 [Accessed July 13, 2020].

47. Markova LI, et al. (2013) Water soluble indodicarbocyanine dyes based on 2,3-dimethyl-3-(4-sulfobutyl)-3H-indole-5-sulfonic acid. *Dyes and Pigments* 96(2):535–546.